UNIVERSITY OF ALBERTA

Gearbox Dynamic Simulation and Estimation of Fault Growth

by

Siyan Wu 

A thesis submitted to the Faculty of Graduate Studies and Research in partial fulfillment of the requirements for the degree of Master of Science

in

Engineering Management

Department of Mechanical Engineering

Edmonton, Alberta

Spring 2007

Your file Votre référence
ISBN: 978-0-494-30041-1
Our file Notre référence
ISBN: 978-0-494-30041-1

ABSTRACT

Gearboxes are among the most important mechanisms in industrial machinery. Monitoring the condition of gearboxes plays an important role in ensuring the reliability and low-cost operation of industrial facilities. One of the most common faults that may develop in a gearbox is a crack in a tooth's root. The appearance and growth of such faults leave signatures in the vibration signals collected from the gearbox. Detection and measurement of these signatures in the early stage are critical for effective fault diagnosis and condition-based maintenance decision making.

This study uses computer simulation to focus on the effects tooth cracks have on the vibration response of a one-stage gearbox with spur gears. The changes in total mesh stiffness caused by a cracked tooth generate periodic impulses in the simulated vibration signal at every meshing period. Various statistical measurements are applied under different signal conditions, their advantages and disadvantages are compared and summarized. Finally, a time domain indicator is improved by applying it to the frequency domain, which has proved to be very sensitive to an incipient tooth crack.

ACKNOWLEDGEMENTS

I wish to express my sincere appreciation to my supervisor, Dr. Ming J. Zuo, for providing me with the opportunity to study in Reliability Research Lab, for guiding my work on an interesting project and research topic, and for his support, advice and encouragement throughout my M.Sc studies.

I would like to thank all the members of the Reliability Research Lab. Their knowledge and ability have given me a new perspective on thinking. Discussions with them have helped me significantly in my work and study.

Special thanks also go to the engineers at Syncrude Research Centre, Mr. Amit S. Aulakh and Dr. Khaled Obaia, who have been excellent models for me of being a professional engineer.

Most importantly, I would like to dedicate this work to my father, Hongzhou Wu, and my mother, Ruyu Shen. Their unconditional love have encouraged me throughout the whole process of pursuing my education and their support has enabled me to bring this work to completion.

Finally, I would like to thank all the people who have helped me during my M.Sc. study at the University of Alberta.

Table of Contents

List of Tables

List of Figures

CHAPTER 1

INTRODUCTION

1.1 Background and Motivation

Gearboxes are among the most important mechanisms in industrial machinery, automotive applications, and in our daily lives. They are widely used to transmit power and produce high rotational speeds and/or change the direction of motion. Because of their growing use in modern technology, gearbox health monitoring and early fault detection have become the subject of intensive investigation and research [36].

Condition monitoring of gearboxes plays an important role in ensuring the reliability and low-cost operation of industrial facilities. The main task of the designer is to select an appropriate gear material and manufacturing technology, combining all the possible factors to insure the high reliability of the gearbox. Even with adequate design, however, the gearbox may still break down eventually. For example, the most common of all failures that cause rotorcraft accidents are failures in the drive train or one of the gearboxes [34]. Since the unexpected failure of a gearbox may cause significant economic loss and even threaten human life, the safety of gearboxes becomes an important factor in mechanical safety. Thus it is necessary to consider proper condition

monitoring so as to give early warning of wear and faults.

Versicherungs [47] found that 60% of gearbox damage is due to faults in the gears, and about 90% of gear faults are due to localized gear damage. Gears generally work in severe conditions. They undergo deterioration of their state, especially on their teeth [14]. There are three categories of gear defects: manufacturing defects (tooth profile error, eccentricity of wheels, etc.), installation defects (parallelism, etc.) and defects appearing during transmission (tooth wear, crack, spalling, etc.). These defects cause transmission error and may lead to gearbox failure [14]. Since the operation of gears always results in repeated loading, this is the main factor that causes the appearance of a fatigue crack in the root of the tooth, thereby reducing structural integrity. Most of the time, a fatigue crack starts from a flaw and may not be considered a serious problem, to begin with. As the tooth crack propagates, however, progressive damage will occur and result ultimately in sudden tooth breakage.

Tooth breakage is the most serious failure for a gearbox [32], one which may lead to the complete failure of the gear. If the fault can be detected early and tracked as it develops, the gear can be replaced before catastrophic failure occurs. Because of its practical importance, crack identification in structures has been the subject of intensive investigation in the last three decades [36].

Many studies have been carried out on machine monitoring in recent years, and the vibration-based technique is manifestly the most commonly used method. The appearance and growth of a gear tooth crack will leave signatures in vibration signals collected from the gearbox. The purpose of this work is to detect and measure such kinds of signatures for effective fault diagnosis and condition-based maintenance decision making.

1.2 Scope and Objectives

The objective of this thesis is to characterize the fault signatures generated by different sizes of fatigue cracks in gearboxes. These signatures can be used to detect the fault at an early stage and track the evolution of its severity.

This study uses computer simulation to study the effects of tooth crack on the vibration response of a one-stage gearbox with spur gears. The total mesh stiffness of a pair of meshing gears is expressed as a function of the rotation angle of the gear, using the so-called potential energy method developed by Yang and Lin [52] in 1987 and refined by Tian [45] in 2004. In Tian's work, a tooth root crack with a specific length is assumed to be present on one of the meshing gears. Since the effect of different crack levels on mesh stiffness and vibration response has not been investigated yet, in this thesis, a range of tooth crack sizes will be assumed and the total meshing stiffness will be calculated. The crack size will be increased incrementally, and the total mesh stiffness under different tooth crack deterioration levels will be calculated. The growing tooth crack causes the total meshing stiffness to change. The total mesh stiffness of the gears is then used in a lumped parameter model to simulate the vibration response of the gears under different deterioration levels of tooth crack.

The changes in the total mesh stiffness caused by the cracked tooth generate periodic impulses in the simulated vibration signal at every meshing period. Impulses are short in duration, but as the faults become more severe, the impulses become stronger. Using the above procedure, a series of vibration signals can be generated through computer simulation. Clearly, it is necessary to detect tooth root cracks as early as possible through scientific methods. In this thesis, we will first apply different statistic indicators to the

original vibration signals in the time domain. Due to the popularity of the use of residual signals in fault diagnosis, two methods of obtaining the residual signal of the original vibration responses will be tried, and then the above statistic indicators will be applied again. The diagnosis resulting from these statistical techniques based on both original signals and residual signals will be compared in the time domain, and the one that can detect the tooth crack earliest will be selected. In addition, the method of calculating kurtosis based on the frequency domain, which was proposed by Dwyer [11] in 1983, will be introduced and applied to the simulated gearbox data. Referring to the testing results, the existing time domain indicator, FGP (fault growth parameter), which was developed by Lin *et al.* in 2004, will be improved by applying it to the frequency domain. Finally, its performance in fault diagnosis will be tested.

1.3 Organization of Thesis

The thesis is organized as follows. Chapter 2 reviews relevant literature surveys establishing mathematical models of gear dynamics and vibration-based analytical techniques for gear fault detection. Chapter 3 summarizes Tian's [45] mesh stiffness model for a gearbox system with a perfect gear pair and gives a cracked tooth model and its influence on mesh stiffness. Chapter 4 presents the results of the dynamic simulation of gearbox system response with and without the tooth root cracks. The effects on the vibration signals of increasing crack levels are also illustrated in this chapter. Chapter 5 is devoted to degradation estimation using statistical techniques based on simulated vibration signals; both time domain and frequency domain signals are employed and the performance levels of the different statistical indicators are

compared. An existing time domain indicator is also improved by being applied to the frequency domain. Finally, Chapter 6 gives the summary and future recommendations.

CHAPTER 2

LITERATURE REVIEW

With the growing focus on gears in industrial machinery, a great deal of research has been undertaken to study the dynamic modelling of gears. Naturally, with the wide use of gearboxes, condition monitoring plays an important role in ensuring the reliability and low-cost operation of industrial facilities. Hence, in this chapter, we will review the literature that provides various mathematical models of gear dynamics and vibration-based techniques for gear fault detection.

2.1 Mathematical Models of Gear Dynamics

Since there are many publications on gear modelling, in this section, we will focus on surveying the mathematical models for gear dynamics. In these models, tooth mesh stiffness is considered as the potential energy-storing element in the system, and the other elements (including shaft and bearings) are considered flexible. If the stiffness of shaft and bearings approximates the tooth mesh stiffness, the vibration coupling of these elements is also included.

Since gear mesh stiffness in engagement is the key element in the analysis of gear dynamics, Kasuba and Evans [23] began in 1981 to use a large

scale digitized approach to calculating gear mesh stiffness. For the purpose of simplification, in many analyses as [40] [46] [7], gear mesh stiffness had been calculated on the basis of assumptions, such as that mesh stiffness was of periodic rectangular, sinusoidal or trapezoidal form. Kasuba and Evans removed this limitation, determining tooth pair mesh stiffness by considering the transmitted load, the number of pairs in contact, gear profile errors, gear hub flexibilities, gear tooth deflections, and the location of contact points. They named their model the variable-variable mesh stiffness model (VVMS). This dynamic model was based on the same coordinates as the earlier static model. A 4th order Runge-Kutta integration scheme as described in reference [17] was used to numerically solve the differential equations of motion. As well, static and dynamic loads, the difference between high contact ratio and normal contact ratio, sliding velocities and the maximum contact pressure acting on the gear teeth as they moved through the contact zone were calculated through a computer program package.

Another key element in gear modelling is determining the dynamic tooth load. In 1985, Kumar, Sankar and Osman [26] used a new state-space method to analyze the dynamic load of spur gear systems. A torsional model which included backlash for a single stage spur gear system was used in their work. They applied the state-space technique to solving their system dynamic equations. Thus, continuous-time state equations were converted to discrete-time state equations and the initial conditions were set at zero and calculated till the end of a mesh cycle. It was observed that by proper selection of the initial conditions, the new straight forward method resulted in considerable savings in computational time. This model was also used to study the variation in dynamic load caused by changes of contact position, operating speed, damp-

ing, system inertias and stiffness, and the stability characteristics of the gear system.

In 1985, Yang and Sun [53] proposed a circular model for studying gear dynamics. By using the kinematic characteristics of the involute curve, they simulated a model for meshing gear systems with backlash. The dynamic equations regarding the gear pair during meshing were dependent on three different geometrical situations and compared the relative displacement between the two meshing tooth profiles along the common tangent line as backlash occurred. In their model, gear meshing stiffness was considered constant and based on the stiffness of Hertzian contact for a single-tooth-pair meshing period. Its value was doubled for a meshing period involving two pairs of teeth, and the energy dissipation during the impact of meshing gears was considered as the damping effect that was proportional to the gear mesh stiffness. Yang and Sun then applied the Runge-Kutta method to the simulation of spur gear dynamics. Three simulation studies were performed, including free vibration, constant load operation, and sinusoidal excitation. They considered that this rotary model was realistic.

Yang and Sun's model was refined by Yang and Lin [52] in 1986 by adding the consideration of bending deflection, axial compression, and Coulomb friction. A frictional force was first added to the original Yang and Sun's rotary model; then, a potential energy method was used to analytically derive the contact force between two meshing gear teeth. The total potential energy stored in the meshing gear system was categorized as either Hertzian, bending or axial compressive energy. To simulate system responses, three types of input torque conditions were used, including zero external torque, constant external torque and sinusoidal external torque. In addition, the importance of bending

deflection, Hertzian deformation, axial compression, Hertzian damping, and friction effect were also compared based on their contributions to dissipated and elastic energies. It was concluded that the improved model contributed to the understanding of the dynamic behaviors of high-speed geared systems.

In 2001, Bartelmus [4] applied mathematical modelling and computer simulation to gearbox dynamic examinations. In his simulation, the factors of design, production technology, operation, and condition change were taken into account. The model for a system with a one-stage gearbox with torsional vibration and wheels in rotary motion was first presented, and then numerical solutions of the differential equations for it were obtained by means of computer simulation. Subsequently, models were developed for a one-stage gearbox system with or without the consideration of inter-tooth friction and both torsional and lateral vibration were included. Finally, a two-stage gearbox system with six torsional degrees of freedom was introduced; for this system, only the torsional vibration and the influence of inter-tooth forces were considered.

Recently, more and more dynamic models are focusing on introducing localized gear faults as an aid to gearbox diagnostics. Kuang and Lin [25] studied the effect of tooth wear on the vibration spectrum variation of a rotating spur gear pair in 2001. In order to approximate the dynamic characteristics of an engaged spur gear pair, the load-sharing alternation, position-dependent mesh stiffness, damping factor, and friction coefficient were considered in the mathematical model. In their model, the mesh stiffness between an engaged gear pair was composed of both Hertzian stiffness and tooth bending stiffness. Localized wear damage was also introduced in their study. The mild wear process in an engaging spur gear pair was simulated based on the wear prediction model proposed by Flodin and Andersson [15], and wear depth was calculated and

updated simultaneously with the dynamic load calculation. Numerical results showed that the velocity and load distribution along the line of action were quite important in determining the sliding wear on the flanks. The transmitted torque amplitude spectrum indicated that the fifth harmonic had a peak amplitude in the frequency band, and the sliding wear introduced after 90,000 and 180,000 operating cycles caused a very slight increase in the peak amplitude while the lower multiples of the mesh frequency increased drastically as sliding wear progressed. These numerical results correlate well with the practical evidence in many published papers.

A simplified spur gear dynamic model involving friction and a crack was developed by Howard *et al.* [21]. Using finite element analysis (FEA), the model incorporated the effect of variations in gear tooth torsional mesh stiffness as gears mesh together. The torsional mesh stiffness, k_m, was considered related to the linear tooth bending stiffness, k_{mb} as $k_m = k_{mb} \times r_b^2$, where r_b represented the base circle radius. The torsional and transverse motions of the gears and shafts were then coupled together. The method of introducing the frictional force between teeth into the dynamic equations was also given. The direction, value and position of the frictional force between the gear teeth had to be determined, then Simulink built upon a MATLAB [37] environment was used to solve the differential equations and simulate the dynamic motion of a 16-degree-of-freedom gearbox system. A 4.7mm gear tooth root crack was introduced by using the FEA model and it was observed that the crack introduced the greatest change in tooth meshing stiffness at the end of the single tooth meshing period.

This section has reviewed various methods of gear dynamic modelling with or without tooth damage. Chapters 3 and 4 utilize the knowledge gained from

the literature to build a gear mesh stiffness model with propagating tooth root crack and to simulate the corresponding system dynamic response that supports the diagnostic signal evaluation for fault detection. First, however, in Section 2.2, we will continue to review existing vibration-based gear fault detection techniques.

2.2 Vibration-Based Analytical Techniques for Gear Fault Detection

There are three main types of approach to the detection of faults in mechanical systems: acoustic signal analysis, debris monitoring, and vibration analysis [50]. Among them, vibration analysis is one of the most powerful tools available for the detection of rotating machinery problems. This is because: first, it has a record of accuracy and reliability; second, different defects produce different vibration patterns; third, vibration monitoring is relatively inexpensive [54].

In Section 2.1, we have already reviewed the various models of gear dynamics. In this section, we will survey the literature on how to detect localized gear faults on the basis of vibration signals. Currently, there are many vibration-based analytical techniques available for identifying gear faults. According to the analysis domain, they can be classified as time domain analysis, frequency domain analysis, and time-frequency analysis. In this section, these various vibration analysis techniques are reviewed.

2.2.1 Time Domain Analysis

Prior to the commercial availability of spectral analysers, almost all vibration analysis was performed in the time domain [16]. The traditional techniques for this are based on statistical measurements of the vibration signal. Therefore,

selecting a proper vibration indicator to reflect the deterioration of the equipment effectively is a critical task in machinery diagnostics. A good indicator is expected to not only distinguish failure conditions from normal conditions by a simple tendency analysis, but also avoid the influence of other different equipment operation parameters. A number of simple signal indicators based on the time domain waveform have widespread application in mechanical fault detection [16].

Indicators which use statistical functions to characterize gear vibration are called "condition indices" in [30]; they process the vibration of a gearbox and return a single value indicating its overall health. Their values are expected to increase with the evolution of fault severity so as to reflect the gearbox's deteriorating condition. Among the existing commonly used statistic indicators, the simplest methods for overall vibration level measurement include peak, root mean square (RMS), and crest factor (CF).

The peak level of the signal is defined simply as half the difference between the maximum and minimum vibration levels, which can be expressed as [16]:

$$\text{peak} = \frac{1}{2}(\max(x(t)) - \min(x(t))) \tag{2.1}$$

where $x(t)$ represents the time domain signal.

The RMS is the normalized second central moment of the signal (standard deviation). For sampled signals, the RMS value is defined as [16]:

$$\begin{aligned} \text{RMS} &= \sqrt{\frac{1}{N}\sum_{n=1}^{N}(x(n) - \bar{x})^2} \\ \bar{x} &= \frac{1}{N}\sum_{n=1}^{N} x(n) \end{aligned} \tag{2.2}$$

where N is the number of samples taken in the signal, $x(n)$ is the amplitude of the signal for the nth sample, and $\bar{x}$ is the mean value of all the amplitudes.

The crest factor is defined as the ratio of the crest value to the RMS of the signal [9]:

$$\text{Crest factor} = \frac{\text{Crest value}}{\text{RMS}} = \frac{\sup|x(n)|}{\sqrt{\frac{1}{N}\sum_{n=1}^{N}[x(n)]^2}} \tag{2.3}$$

where $\sup|x(n)|$ represents the maximum absolute value of the signal. Thus, the presence of high-amplitude peaks may lead to a high crest factor.

In the past few years, higher order statistics are garnering more intensive interest, and kurtosis is the most basic tool among them. The successful use of kurtosis has been reported for bearing condition monitoring since its independence of operating conditions [42]. It is considered a normalized form of the fourth central moment of a given sampled signal $x(n)$, which is given by [9]:

$$\text{kurtosis} = \frac{\frac{1}{N}\sum_{n=1}^{N}(x(n)-\bar{x})^4}{[\frac{1}{N}\sum_{n=1}^{N}(x(n)-\bar{x})^2]^2}. \tag{2.4}$$

Because of the use of the fourth power, kurtosis is very sensitive to the peakedness of the signal. If the signal is modified by a small number of high peaked impulses, the corresponding kurtosis will be high.

For a normal distribution signal, the kurtosis value will be approximately 3. A lower kurtosis value represents a flat distribution, while a higher value represents a peaked distribution. Any increase in kurtosis from a value of 3 indicates how far outlying data points are from the mean [39].

Dyer *et al.*[13] were among the pioneers who applied kurtosis to fault diag-

nosis. A series of statistical moments are discussed; among them, the normalized fourth moment, kurtosis, represents a compromise measure between the insensitive lower moments and the over-sensitive higher moments. To observe how kurtosis predicts the condition of rolling element bearings, it is tested by measuring the bearing housing vibration. Experimental signals have been employed to prove the variation of kurtosis in different frequency bands with advancing damage. If all the values are close to 3, the bearing is undamaged; an increase from 3 signifies damage, and its extent can be determined. It has also been found that, unlike the other measurements such as RMS, peak, power spectral density and shock pulse, kurtosis is insensitive to changes in load and speed for an undamaged bearing. Finally, this technique has been proved to be applicable to all types of rolling element bearings by tests in both the laboratory and the field [13].

Although kurtosis is a very popular statistical indicator, it is actually not well understood and many misconceptions are not widely recognized. DeCarlo [8] confirmed the meaning of kurtosis and clarified some confusions concerning it in 1997. He emphasized that peakedness and tailedness are both components of kurtosis. He also distinguished between kurtosis and variance, noting that kurtosis reflects the shape of a distribution, and so is not affected by variance. Decarlo's paper explained how to use kurtosis, pointing out its robustness in assessing normality, its use for detecting outliers, and its use as a generalized test and estimator.

In addition to the above commonly used indicators, other statistical measures have been developed by researchers. In [31], Lin *et al.* proposed a new indicator, which is so-called FGP (Fault Growth Parameter); its revised version FGP1 measures the whole course of gear tooth damage evolution. FGP

and FGP1 were expected to be indicators that increase robustly with fault deterioration levels. FGP is defined as the part (percentage of points) of the residual error signal, which exceeds three standard deviations calculated from the baseline residual error signal taken when the experiment began, or

$$\text{FGP} = 100 \sum_{i=1}^{L} \frac{1}{L} I(r_i > \overline{r} + 3\sigma_0), \tag{2.5}$$

where r_i is the current residual error signal at point i, $\overline{r}$ is the mean value of the current residual signal, σ_0 is the "baseline" standard deviation and I(.) is the indicator function. Here the current signal represents the one that is waiting to be tested to determine the health of the gearbox, and the baseline standard deviation is derived from the known signal that is collected under normal operating conditions. As to the residual error signal, it is obtained by a signal processing algorithm developed at Penn State University Applied Research Laboratory (ARL) [39]. FGP and FGP1 can, however, simply be applied to a raw signal or a signal already put through other filtering methods.

In the same paper, the revised version, FGP1, is defined as the weighted part (weighted percentage of points) of the residual error signal, which exceeds three standard deviations from the baseline residual error signal, or

$$\text{FGP1} = 100 \sum_{i=1}^{L} \frac{w_i}{W} I(r_i > \overline{r} + 3\sigma_0) \tag{2.6}$$

where $w_i = I(r_i \leq \overline{r} + 3\sigma_0) + (\lfloor \frac{r_i - \overline{r}}{3\sigma_0} - 1 \rfloor + 1)$, $W = \sum_{i=1}^{L} w_i$, and $\lfloor \cdot \rfloor$ is the floor function.

Lin *et al.* [31] claimed that both the FGP and FGP1 provide a clear way to track the development of cracks (or spalls) in gear teeth, with FGP1 being more sensitive to problems.

In [2], the Kolmogorov-Smirnov (KS) test was introduced to monitor spur gears' vibration condition. This technique is based on a statistical comparison of two time-domain vibration signatures. The main idea of the KS test was to compare the cumulative distribution function (CDF) of two vibration signatures, which, if working under the same gear condition, must have identical CDF values. If damage was present and strong enough, it would cause variations in the CDF of the vibration signature. When comparing it with a perfect gear vibration signature, any difference can be attributed to gear faults. Consequently, when a number of known-conditions gear vibration signatures were compared with an unknown vibration signature, it was possible to judge the most likely condition of the undiagnosed gear. In this paper, The KS test was applied to both numerical and experimental signals. It was shown that this method could be used, not only for the identification of early tooth fatigue cracks on gears but also, for the estimation of fault advancement.

2.2.2 Frequency Domain Analysis

Frequency domain analysis is also a classical vibration analysis tool. It has been proved to be a valuable tool for detection and basic diagnosis of faults in simple rotating machinery [16]. Using frequency analysis, a complex signal can be broken down into various frequency components; it is easy for analysers to focus on those that are valuable in fault diagnosis. The mathematical basis of frequency analysis is the Fourier Transform (FT), which is expressed as [41]:

$$X(f) = \int_{-\infty}^{\infty} x(t) e^{-j2\pi ft} dt \tag{2.7}$$

where $x(t)$ represents a continuous time domain signal, $X(f)$ is the spectrum of $x(t)$ and $j = \sqrt{-1}$. Since all signals in a digital computer are discrete in

nature, the transform must be calculated at each discrete point. This is called the discrete Fourier transform (DFT), which is obtained by [6]:

$$X(k) = \sum_{n=0}^{N-1} x(n) e^{-j\frac{2\pi kn}{N}}, 0 \leq k \leq N-1 \tag{2.8}$$

where $x(n)$ is a sampled time domain signal that is quantized in time as

$$x(n) = x(t)|_{t=nT_s} \tag{2.9}$$

where n is an integer and T_s is some constant time interval.

Equation (2.8) is called the N-point DFT of the sampled signal $x(n)$. For each value of k, the value of $X(k)$ represents the Fourier transform at the frequency $\omega = \frac{2\pi}{N}k$.

In practice, to calculate the discrete Fourier transform (DFT) more efficiently, a so-called fast Fourier transform (FFT) algorithm is usually applied. Traditionally, one major use of the FFT is to do the spectrum estimation. For a given signal, the power spectrum estimation shows the signal's power at given frequency bins in the frequency domain. As illustrated in [41], the power spectrum, $S_{AA}(f)$, of a time signal, $x(t)$, is given by:

$$S_{XX}(f) = |\mathrm{FT}[x(t)]|^2 \tag{2.10}$$

where FT is the Fourier transform. In conventional signal processing applications, the estimation of the power spectrum is a well-known and often employed method.

Cepstral analysis is also a widely used tool in gear diagnostics. The power cepstrum theory was first introduced by Bogert *et al.* in 1963 and it is defined as the "inverse Fourier transform of the log of the spectrum" [1]. The power

cepstrum of the time domain signal, $x(t)$, can be expressed as follows [41]:

$$C_{XX}(\tau) = \mathrm{FT}^{-1}[\log S_{XX}(f)]. \tag{2.11}$$

The unique feature of cepstrum is the logarithm conversion of the original spectrum. The cepstrum is used to determine periodicity in a spectrum and indicate the gear-meshing sidebands [42], which can not be achieved by spectrum estimation alone. In gear vibrations, the presence of sidebands can give information about the damage of components. Thus, the cepstrum can be applied to machine diagnostics.

Currently, most gear fault diagnostic techniques are based on the residual signal [51]. For healthy gears, the gear-meshing frequency and its harmonics that constitute what is called the regular signal dominate the meshing vibration spectrum [51]. This part of the signal, the regular component, becomes redundant for fault detection; therefore, removing the fundamental and harmonics of the tooth-meshing frequency from the raw signal results in a signal containing more obvious information that is directly related to gear faults, and the kurtosis level increases routinely with fault evolution.

As summarized in [56], a difference signal is generated by removing the regular meshing components, including the shaft frequencies and their harmonics, the meshing frequencies and their harmonics, and all first-order sidebands. When that is done, the kurtosis of the difference signal is called "FM" as shown below:

$$\mathrm{FM4} = \frac{N\sum_{n=1}^{N}(d(n)-\overline{d})^4}{[\sum_{n=1}^{N}(d(n)-\overline{d})^2]^2} \tag{2.12}$$

where $d(n)$ is the amplitude of the difference signal for the nth sample, and $\bar{x}$

is the mean value of all the amplitudes.

Similarly, a residual signal can be obtained by removing the shaft frequencies and their harmonics, and the meshing frequencies and their harmonics. The only difference between the residual signal and the difference signal is that the residual signal includes the first-order sidebands while the difference signal does not. Applying kurtosis to the residual signal, it becomes a new indicator, "NA4".

In addition to FM4 and NA4, there exist several indicators involving kurtosis parameter applications such as FM4*, NA4, NB4, and NB4* [42]. Each has its own advantage over the others.

2.2.3 Time-Frequency Domain Analysis

During the last decade, some time-frequency methods have received growing attention and have gained acceptance in the field of condition monitoring [5]. Instead of traditional time domain analysis and frequency domain analysis, the combination of time and frequency analysis is employed and is gradually becoming a popular trend in gear fault diagnosis. Representing the signal properties in both the time and frequency domains simultaneously provides a powerful advantage in examining non-stationary vibration signals that can easily be interpreted. The local features of a signal can easily be characterized, and all components in the frequency range of interest, their sequences, causality and changes with time can be displayed on a single chart [48].

Short-time Fourier transform (STFT) is a classic method of time-frequency analysis. If the spectrum of a signal, $x(t)$, varies with time, we may apply a window function to $x(t)$ to demonstrate how the signal frequency changes over time; this cannot be achieved by the Fourier transform. The STFT is defined

as [19]:

$$S(b,\omega) = \int_{-\infty}^{\infty} w^*(t-b)x(t)e^{-j\omega t}dt \tag{2.13}$$

where $w(t)$ is the window function and * designates the complex conjugate. w^* is seen to be the mirror image of w around the real axis, thus, the real parts and amplitudes of w and w^* have the same sign while the imaginary parts and phase angles have opposite signs, i.e., if $w = x + yi$, $w^* = x - yi$. b is the translation parameter which indicates where the window is located, and ω represents the frequency scale. The magnitude squared of the STFT is called the spectrogram, which can be expressed as $|S(b,\omega)|^2$. The three-dimensional plot of $|S(b,\omega)|^2$, time scale b and frequency scale ω shows how the energy of the process is decomposed over time and frequency.

Another technique that plays a central role in time-frequency analysis is known as the time-frequency distribution. The pioneer time-frequency distribution is the Wigner-Ville distribution, which originated in quantum mechanics in 1932 and was applied to signal processing and spectral analysis in 1948. There exist, however, various distributions, including spectrogram, Pseudo-Wigner distribution (PWD), Choi-Williams distribution, Cone-kernel distribution, and reduced interference distribution [19].

Wang *et al.*[48] applied the spectrogram to calculating the time-frequency distribution of a gear vibration signal in early gear failure detection. Since the changes caused by damage appeared in the vibration signal only when the affected teeth were in mesh, the periodical impulses were of short duration and their corresponding magnitude was, at first, very small. How to recognize when this limited energy developed in the vibration signal as a result of damage become the most important task in fault diagnosis and condition

monitoring. The spectrogram showed the squared magnitude of the short-time Fourier transform (STFT). By applying the spectrogram to the vibration signal, the local power spectral density could be given in the time-frequency domain, which represents the energy distribution across the frequency spectrum as a function of time. For the purpose of early detection, Gaussian function was found to be the most suitable window; it could not only emphasize the change in the signal due to damage, but also make the time-frequency distribution clearer and easier to interpret. To demonstrate the spectrogram, the numerically simulated signal and experimentally measured time domain averages of the vibration signal from one of a series of large reduction gearboxes were employed. In both examples, the spectrogram gave a clear time-frequency distribution of the energy; as well, the specific time and frequency components related to gear damage could be determined with a great deal of sensitivity.

Recently, wavelet transform (WT) is attracting considerable interest with regard to detecting transient and non-stationary vibration signals. Compared to STFT, WT is more suitable for wideband systems, in which the bandwidth is much greater than the central frequency. WT originated in the early 1980s and is becoming a powerful signal processing tool for detecting both the time and frequency characteristics of vibration signals. The wavelet transform of a signal, $x(t)$, is defined in the time-frequency domain as [14]:

$$W(a,b) = \frac{1}{\sqrt{|a|}} \int_{-\infty}^{\infty} x(t) q^*(\frac{t-b}{a}) dt, \tag{2.14}$$

where $q(t)$ represents the wavelet function and * designates a complex conjugate. The scale parameter, a, determines the width or scale of the wavelet function, and the translation parameter, b, determines its position.

A great deal of research has been done on the wavelet transform in machin-

ery diagnostics. Wang *et al.*[49] outlined the definition of the wavelet transform and suggested its application to gearbox vibration signals for fault detection. They indicated that any gear damage may cause a relatively brief transition in the vibration, for different types of damage, the duration was also different. In contrast to the time-frequency distribution, the WT used a changing window width function, which made it possible to display all the sections of the signal simultaneously. Wang *et al.* employed the time-frequency damage detection method using the wavelet transform; the calculation could be done easily by taking advantage of the FFT algorithm. In particular, they tested the wavelet transform using the vibration signal obtained from a helicopter's main rotor gearbox undergoing a fatigue test in a full-scale gearbox test facility. A Gaussian-enveloped oscillation wavelet was applied and the absolute values of the wavelet transform were presented. On the time-scale distributions, both small and large variations in the vibration signal were successfully detected, showing not only tooth damage but also normal manufacturing errors.

Lin and McFadden [33] introduced a linear wavelet transform, "LWT", concept to obtain a time-frequency spectrogram of gear vibration signals. The LWT could be calculated simply through the fast Fourier transform by filtering the signal spectrum with wavelet filters. By locating the centers of daughter wavelet filters from a range of lower to higher channels, the high-frequency components could be caught; this made it easier to detect the transient signal. Linear wavelet transform was applied, based on the B-spline wavelet in order to decompose exactly the spectrum of a complex signal. This model resulted in an acceptable time and frequency resolution; a tradeoff makes it possible to analyze signal properties in the time and frequency domains concurrently. The spectrogram distribution revealed in the vibration signal the sidebands of the

dominant tooth-meshing harmonic, generated by the gear fault. Experimental data was employed to test this method. Four of the demodulated signals were processed by the cubic B-spline wavelet-based LWT; finally, the location of the fatigue crack was detected. Also, by comparing the spectrograms over a period of time, the growth of the crack could be monitored.

2.2.4 Comparison

Based on the surveys of vibration-based fault diagnostic techniques, it has been concluded that time domain analysis is the most simple, fast and inexpensive means of damage detection. It is also convenient for on-line monitoring; however, it is not sensitive enough to identify the different kinds of machinery faults. Both time domain analysis and frequency domain analysis have a common shortcoming – their difficulty in detecting non-stationary signals; this is the purpose for which time-frequency domain analysis was initiated. The idea of expressing the frequency components in the time scale has been investigated significantly in the last two decades; its main disadvantage lies in its complexity.

2.3 Summary

In light of the aforementioned literatures, we have reviewed the current mathematical models of gear dynamics and main vibration-based fault diagnosis techniques. Because of the tremendous usage of gears in numerous industrial applications, the health monitoring of gears has been studied extensively. Our literature review shows that a considerable amount of research has been done on gearbox dynamic responses affected by localized gear faults, in an attempt to find viable vibration-based fault detection techniques. From Section 2.2, it

can be seen that statistic measure is one of the most commonly used methods, and quite a few statistic indicators have been recommended for use in gear fault detection. Thus, in this thesis, we will test the performance of the indicators reviewed in Section 2.2 and compare their advantages and disadvantages based on computer-simulated gearbox vibration signals. Referring to the test results, we will improve the indicator FGP (Fault Growth Parameter) in order to better accomplish its purpose of early fault detection.

Since the mesh stiffness is a primary source of gear vibration, in order to simulate the dynamic responses of gearboxes with or without fatigue cracks, we will, in Chapter 3, first derive the time-varying mesh stiffness of perfect gear pairs based on the potential energy method developed by Yang and Lin [52]. Then, a fatigue crack will be initiated in one of the pinion tooth roots and its influence on mesh stiffness will be studied.

Chapter 3

Modeling of Gear Mesh Stiffness When a Tooth is Cracked

In Chapter 2, a number of gear dynamic models were reviewed. In this chapter, we will first summarize the mesh stiffness model of the gearbox system with a perfect gear pair as reported by Tian [45], and then a propagating tooth root crack will be introduced and its influence on mesh stiffness will be described.

3.1 Method of Calculating the Mesh Stiffness of Sound Gears

Today most gears used in industry are of involute tooth profile [53]. For that reason, an involute spur type gear pair is considered in this thesis. For machinery diagnosis and early fault detection, it is very necessary to establish the dynamic model of the gear transmission both with perfect teeth and with defective teeth. Since the time varying mesh stiffness is the main cause of gear vibration, first we study the method of calculating the mesh stiffness of sound gears.

There is a vast amount of literature on gear mesh stiffness modelling; the model described within this study is based on the one developed by Yang and Lin [52] in 1987. They proposed using the potential energy method to analyt-

ically model the effective mesh stiffness. In their model, the only compliance considered is due to the gear tooth; all other elements have been assumed to be perfectly rigid. Yang and Lin have pointed out that the total potential energy stored in the meshing gear system includes three components: Hertzian energy, bending energy, and axial compressive energy. This model was refined by Tian [45] in 2004 at which time shear energy was taken into account as well. In the following, we summarize the results reported by [52] and [45] on a perfect pair of gears.

The total effective mesh stiffness of a gear tooth is composed of Hertzian contact stiffness, bending stiffness, shear stiffness and axial compressive stiffness, which can be obtained by [45]:

$$k_t = \frac{1}{\frac{1}{k_h} + \frac{1}{k_{b1}} + \frac{1}{k_{s1}} + \frac{1}{k_{a1}} + \frac{1}{k_{b2}} + \frac{1}{k_{s2}} + \frac{1}{k_{a2}}} \tag{3.1}$$

Hertzian contact stiffness is a constant during the meshing period, which can be expressed as [53]:

$$k_h = \frac{EL\pi}{4(1-\nu^2)} \tag{3.2}$$

where E, L, ν represent Young's modulus, tooth width, and Poisson's ratio respectively.

Bending stiffness, k_b, shear stiffness, k_s, and axial compressive stiffness, k_a, can be derived by:

$$k_b = \frac{F^2}{2U_b} \tag{3.3}$$

$$k_s = \frac{F^2}{2U_s} \tag{3.4}$$

$$k_a = \frac{F^2}{2U_a} \tag{3.5}$$

where F is the elastic contact force between two meshing gear teeth, and U_b, U_s, U_a represent bending energy, shear energy, and axial compressive energy respectively. By using the property of involute curve, it is possible to see that the elastic contact force, F, is always along the action line, as shown in Figure 3.1. This force can be decomposed into F_a (which is parallel to the tooth's central line) and F_b (which is perpendicular to that line).

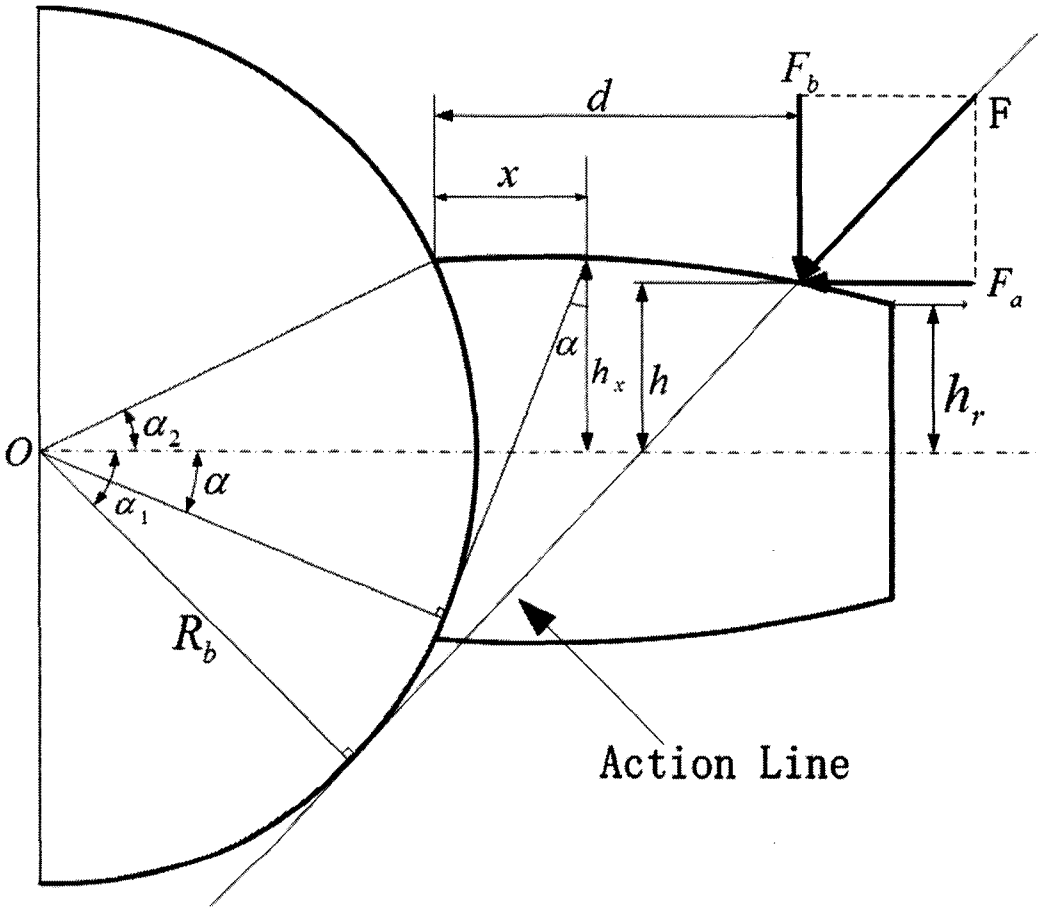

Figure 3.1: Elastic force on a gear tooth [45]

The bending effect caused by F at the section where the distance from the tooth root is x is:

$$M = F_b(d - x) - F_a h \tag{3.6}$$

where d represents the distance between the contact point and the tooth's root, and h represents the distance between the contact point and the tooth's central line. Based on the property of involute curve, x, d, and h can be calculated from the following equations [52]:

$$x = R_b[\cos\alpha - (\alpha_2 - \alpha)\sin\alpha - \cos\alpha_2] \tag{3.7}$$

$$d = R_b[(\alpha_1 + \alpha_2)\sin\alpha_1 + \cos\alpha_1 - \cos\alpha_2] \tag{3.8}$$

$$h = R_b[(\alpha_1 + \alpha_2)\cos\alpha_1 - \sin\alpha_1] \tag{3.9}$$

where R_b is the base circle radius of the gear, α_1 is the angle between the line O_1C and the tooth's central line, and α_2 is the half of the base tooth angle. Angle α_2 can be related to the number of gear teeth, N, and the pressure angle, α_0, as:

$$\alpha_2 = \frac{\pi}{2N} + \tan\alpha_0 - \alpha_0. \tag{3.10}$$

The axial compressive effect is totally provided by F_a and the shear effect is totally provided by F_b; they can be expressed as:

$$F_a = F\sin\alpha_1 \tag{3.11}$$

$$F_b = F\cos\alpha_1. \tag{3.12}$$

Therefore, the potential energy stored in a meshing gear tooth can be calculated by [45]:

$$U_b = \int_0^d \frac{M^2}{2EI_x}\mathrm{d}x = \int_0^d \frac{[F_b(d-x) - F_a h]^2}{2EI_x}\mathrm{d}x \tag{3.13}$$

$$U_s = \int_0^d \frac{1.2F_b^2}{2GA_x}\mathrm{d}x = \int_0^d \frac{[1.2F\cos\alpha_1]^2}{2GA_x}\mathrm{d}x \tag{3.14}$$

$$U_a = \int_0^d \frac{F_a^2}{2EA_x}\mathrm{d}x = \int_0^d \frac{[F\sin\alpha_1]^2}{2EA_x}\mathrm{d}x \tag{3.15}$$

where I_x and A_x represent the area moment of inertia and area of the section where the distance from the tooth's root is x, and G represents the shear modulus. They can be obtained by:

$$\begin{aligned} I_x &= \frac{1}{12}(2h_x)^3 L = \frac{2}{3}h_x^3 L \\ &= \frac{2}{3}R_b[(\alpha+\alpha_2)\cos\alpha - \sin\alpha]^3 L \end{aligned} \tag{3.16}$$

$$A_x = 2h_x L = 2R_b[(\alpha+\alpha_2)\cos\alpha - \sin\alpha]L \tag{3.17}$$

$$G = \frac{E}{2(1+\nu)} \tag{3.18}$$

where h_x represents the distance between the point on the tooth's curve and the tooth's central line where the horizontal distance from the tooth's root is

x.

Substituting Equations (4.2) - (3.18) into Equations (3.3), (3.4), and (3.5), we derive the bending stiffness, shear stiffness, and axial compressive energy as the following [45]:

$$\frac{1}{k_b} = \int_{-\alpha_1}^{\alpha_2} \frac{31 + \cos\alpha_1[(\alpha_2 - \alpha)\sin\alpha - \cos\alpha]^2(\alpha_2 - \alpha)\cos\alpha}{2EL[\sin\alpha + (\alpha_2 - \alpha)\cos\alpha]^3} \mathrm{d}\alpha \tag{3.19}$$

$$\frac{1}{k_s} = \int_{-\alpha_1}^{\alpha_2} \frac{1.2(1+\nu)(\alpha_2 - \alpha)\cos\alpha(\cos\alpha_1)^2}{EL[\sin\alpha + (\alpha_2 - \alpha)\cos\alpha]} \mathrm{d}\alpha \tag{3.20}$$

$$\frac{1}{k_a} = \int_{-\alpha_1}^{\alpha_2} \frac{(\alpha_2 - \alpha)\cos\alpha(\sin\alpha_1)^2}{2EL[\sin\alpha + (\alpha_2 - \alpha)\cos\alpha]} \mathrm{d}\alpha. \tag{3.21}$$

So far, the procedure for obtaining the total effective mesh stiffness of a pair of perfectly meshing gear teeth has been illustrated; k_t can be expressed as the functions of angular variable α_1 as shown in Equation (3.1), and the subscripts 1 and 2 represent the pinion and the gear respectively.

During the gears' meshing period, however, the number of pairs of meshing teeth alternates between one and two. For the single-tooth-pair meshing duration, the total effective mesh stiffness can be calculated according to Equation (3.1); for the double-tooth-pair meshing duration, the total effective mesh stiffness is the sum of the two pairs' stiffnesses, which is shown as [45]:

$$k_t = \sum_{i=1}^{2} \frac{1}{\frac{1}{k_{h,i}} + \frac{1}{k_{b1,i}} + \frac{1}{k_{s1,i}} + \frac{1}{k_{a1,i}} + \frac{1}{k_{b2,i}} + \frac{1}{k_{s2,i}} + \frac{1}{k_{a2,i}}} \tag{3.22}$$

where i=1 represents the first pair of meshing teeth and i=2 represents the second.

In [45], Tian also derived the calculation expressions of mesh stiffness for the double/single-tooth-pair meshing durations. Assuming the system starts with the initial double-tooth-pair meshing point, the period before the second pair of mating teeth separate is called the double-tooth-pair meshing duration, θ_d. Then, the single-tooth-pair meshing period begins and its duration is called θ_s. One θ_d and one θ_s constitute one meshing period. Because there are 19 teeth on the pinion ($N_1 = 19$), one shaft period is comprised of 19 periodical meshing periods, and each meshing period is equal to $2\pi/N_1$. Therefore, according to Tian's results, the double-tooth-pair meshing duration, θ_d, can be calculated as [45]:

$$\theta_d = \tan(\arccos\frac{N_1\cos\alpha_0}{N_1+2}) - \frac{2\pi}{N_1} - \tan\Delta \tag{3.23}$$

where Δ is equal to

$$\arccos\frac{N_1\cos\alpha_0}{\sqrt{(N_2+2)^2+(N_1+N_2)^2-2(N_2+2)(N_1+N_2)\cos(\arccos\frac{N_2\cos\alpha_0}{N_2+2}-\alpha_0)}}. \tag{3.24}$$

Consequently, the single-tooth-pair meshing duration, θ_s, within one mesh period can be calculated by

$$\theta_s = \frac{2\pi}{N_1} - \theta_d. \tag{3.25}$$

Based on the aforementioned procedure, and using the gear system parameters shown in Table 3.1, MATLAB programs were written to obtain the numerical solution of the total effective mesh stiffness, and the results within one shaft period are displayed in Figure 3.2. It can be observed that for a

Table 3.1: Main parameters of the gear and pinion [45]

Young's modulus	$E = 2.068 \times 10^{11} Pa$
Paisson's ratio	$\nu = 0.3$
Pressure angle	20^o
Diametral pitch	$P = 8 inch^{-1}$
Width of teeth	$L = 0.016m$
Number of teeth on pinion	$N_1 = 19$
Number of teeth on gear	$N_2 = 48$

single meshing period, there are two stages. At first, two pairs of gear teeth mesh together, and the mesh stiffness varies around 1×10^9; then, after the double-tooth-pair meshing duration, the value of the mesh stiffness suddenly suffers a great drop at a certain angular displacement which represents the transition point from double-tooth-pair mesh to single-tooth-pair mesh. After the single-tooth-pair meshing duration, there is a reversion and another identical meshing period starts.

The results of the simulation can be validated by comparing our Figure 3.2 with Figure 3.3 that was generated by Tian in [45]. Though we do not have the numerical values for the tooth mesh stiffness simulated by Tian, Figure 3.2 and Figure 3.3 look identical. Visual observation validates the correctness of our simulation results.

3.2 A Cracked Tooth Model

With the model given in section 3.1, mesh stiffness is expressed as a time varying parameter that reflects the number of meshing gear teeth and the tooth meshing point at different angular displacements. When localized gear faults appear, total mesh stiffness suffers a local reduction during a shaft period. Since tooth crack is one of the most common faults that can develop in a

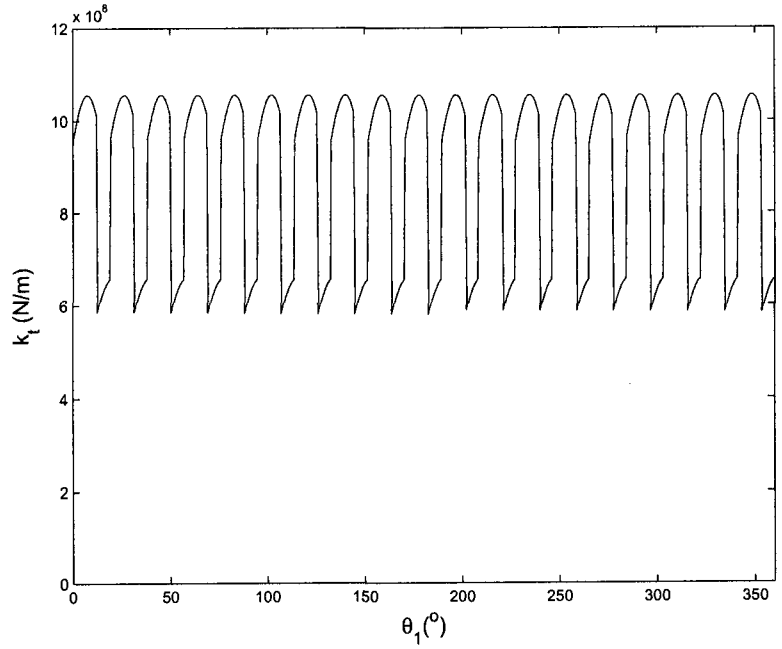

Figure 3.2: The total effective mesh stiffness, k_t, vs. the pinion's angular displacement, θ_1, within one shaft period

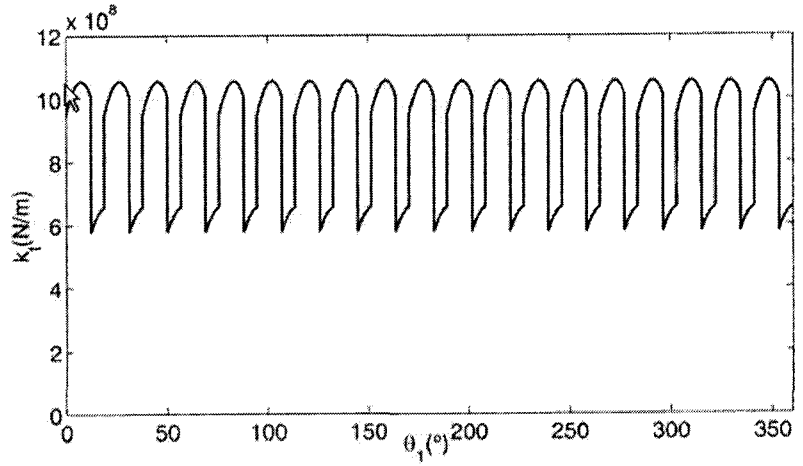

Figure 3.3: The total effective mesh stiffness, k_t, vs. the pinion's angular displacement, θ_1, within one shaft period provided by Tian in [45]

gearbox, in this thesis, the localized defect is assumed to be a crack made in one tooth. To demonstrate how the presence of a fatigue crack influences mesh stiffness, a cracked tooth model needs to be established.

Based on a literature review, [27] [5] [38] [55] , most reported experiments focus on faults in pinions, therefore, we also consider that the crack is located in a single tooth root of a pinion. A tooth root crack typically starts at the point of the largest stresses in the material. According to Figure 3.4, fatigue crack initiation is more likely to be in the critical area of the tooth root, which is on the tensile side of the contact force, F.

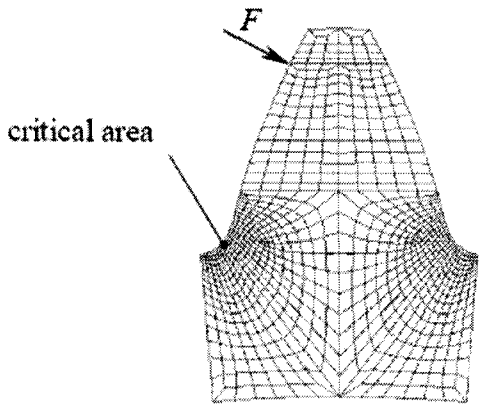

Figure 3.4: Fatigue crack initiation [22]

Much research has been done on the crack propagation path. In [24], a computational model which applied the principles of linear elastic fracture mechanics was used to simulate gear tooth root crack propagation, and the left side of Figure 3.5 shows the numerically determined crack propagation path provided by that study. Studies indicate that crack propagation paths are smooth, continuous, and, in most cases, rather straight with only a slight curvature [28]. Based on the computational results obtained in [24], the crack

propagation path is a slight curve extending from the tooth root. To simplify the crack model, here, we will approximate the shape of the crack as a straight line as shown in the right side of Figure 3.5.

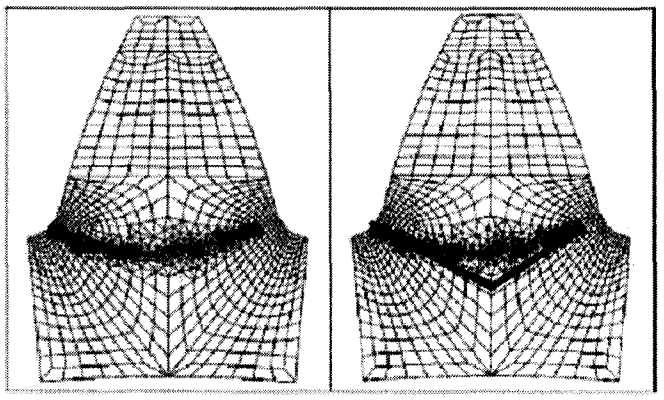

Figure 3.5: Predicted crack propagation path

As shown in Figure 3.6, the shape of the crack can be described in three dimensions: the crack's length, width and thickness. Here, to simplify the model, we focus only on the crack's development in one dimension, so the crack is assumed to be along the whole width of the tooth from the point of its initiation, and the influence of the crack's thickness is ignored. As a result, the complete tooth crack models with full-length development are given in Figures 3.7 to 3.11.

Assume the crack started at the root of the pinion and then proceeded along the normal line of the tooth's root curve. The intersection angle, υ, between the crack and the central line of the tooth is set at a constant 45^o. The crack length, q_1, starts at 0.1mm, and the increment size, Δq_1, is also 0.1mm until the crack reaches the tooth's central line. At that point, q_1 reaches its maximum value, which can be obtained by:

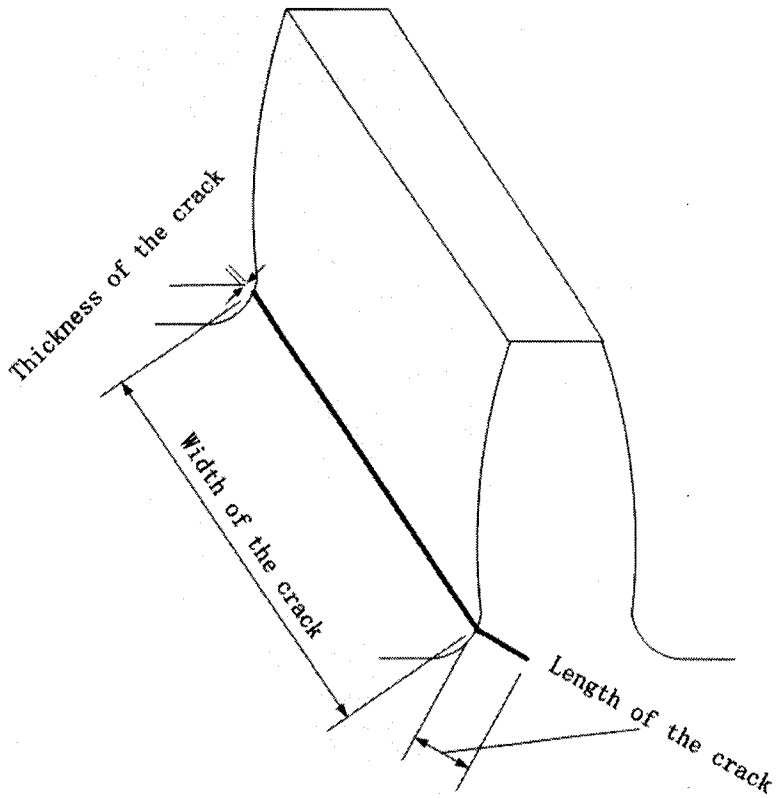

Figure 3.6: A three-dimensional crack

$$q_{1max} = \frac{R_{b1} \sin \alpha_2}{\cos \upsilon} \tag{3.26}$$

where R_{b1} represents the radius of the pinion's base circle.

The crack then changes direction to q_2, which is assumed to be exactly symmetric with q_1 along the tooth's central line. The maximum length of q_2 should be the same as q_1, however, the tooth is supposed to suffer a sudden breakage before the crack runs throughout the whole tooth. Thus the maximum length of q_2 is assumed to be 60% of q_{1max} and the increment size, Δq_2, is 0.1mm.

3.3 Method of Calculating the Mesh Stiffness of a Pinion with a Cracked Tooth

Based on the work with a cracked tooth summarized in Section 3.1, Hertzian and axial compressive stiffnesses remain the same as in the perfect gear. Referring to Equation (3.2), since the width of the tooth, L, doesn't change, and the other parameters are all constant values, Hertzian stiffness remains the same. As for axial compressive stiffness, upon mechanical analysis, it is obvious that the tooth's root crack will not influence the section's strength in bearing axial compressive force, and the stiffness can still be derived by Equation (3.21). The bending and shear stiffnesses will change, however, due to the appearance of the crack. According to the same procedure used in deriving the bending and shear stiffnesses of perfect meshing pairs, the cracked tooth's bending and shear stiffnesses can be obtained as follows.

Referring to Figure 3.8, R_{O_1}, R_{O_2}, R_{b1} and R_{b2} represent the radius of the pinion's and the gear's outside circle and base circle respectively. They can be expressed as [45]:

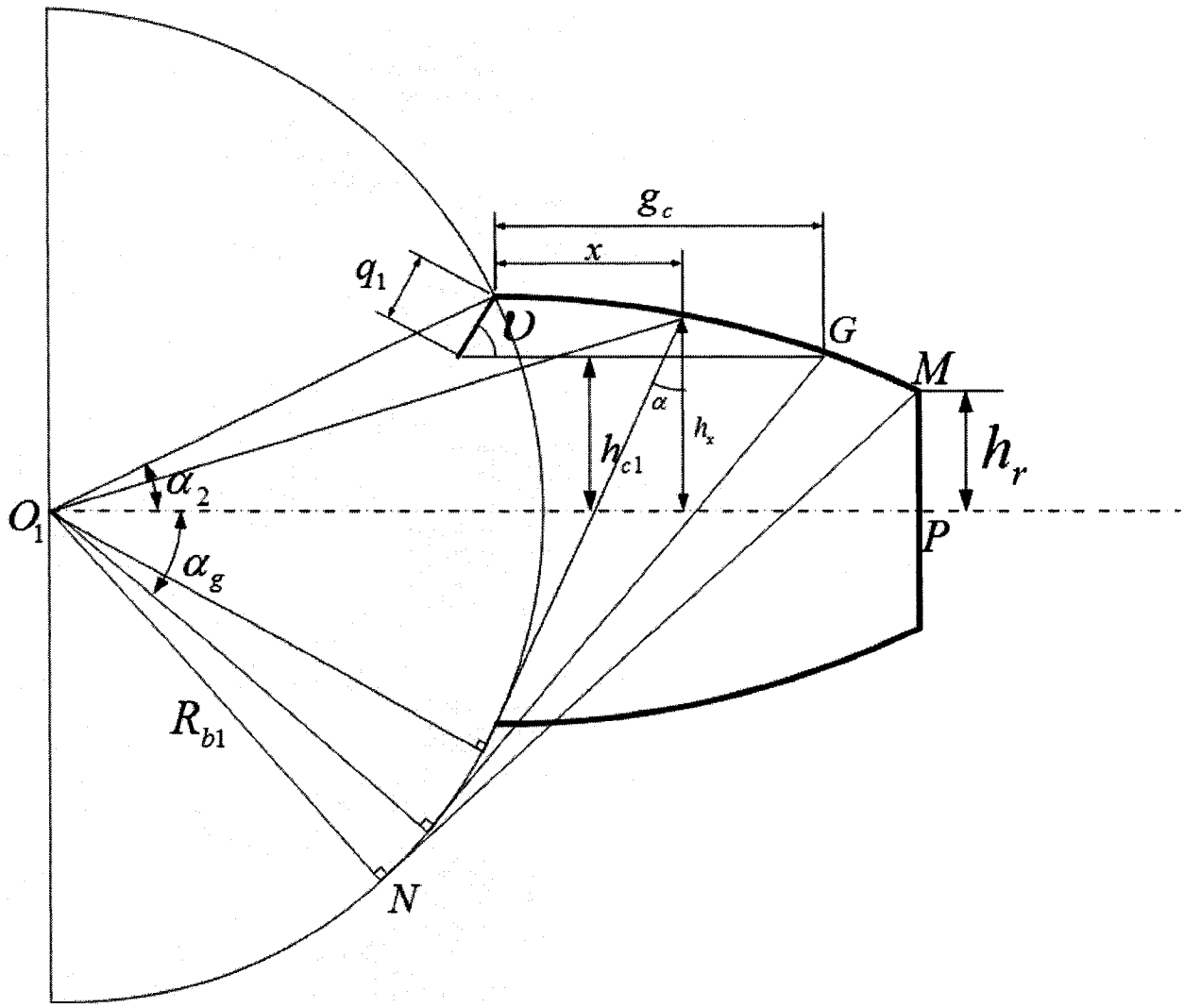

Figure 3.7: A cracked tooth model for **Case 1**

$$R_{O_1} = \frac{N_1 + 2}{2P} \tag{3.27}$$

$$R_{O_2} = \frac{N_2 + 2}{2P} \tag{3.28}$$

$$R_{b1} = \frac{N_1}{2P} \cos \alpha_0 \tag{3.29}$$

$$R_{b2} = \frac{N_2}{2P} \cos \alpha_0. \tag{3.30}$$

Then half of the roof chordal tooth thickness, h_r, can be calculated by:

$$h_r = R_{b1} \times [(\angle \mathrm{PO_1N} + \alpha_2) \cos(\angle \mathrm{PO_1N}) - \sin(\angle \mathrm{PO_1N})] \tag{3.31}$$

where $\angle \mathrm{PO_1N}$ can be obtained by Equation (3.32)

$$\mathrm{MN} = \sqrt{R_{O1}^2 + R_{b1}^2} = R_{b1} \times (\angle \mathrm{PO_1N} + \alpha_2). \tag{3.32}$$

For a given crack length, q_1, as shown in Figure 3.7, h_{c1} represents the vertical distance between the tip of the crack and the tooth's central line, which corresponds to the angle α_g. According to the geometry of the involute tooth, h_{c1} can be calculated by:

$$h_{c1} = R_{b1} \sin \alpha_2 - q_1 \sin \upsilon. \tag{3.33}$$

Then comparing the values between h_{c1} and h_r, the cracked tooth's bending and shear mesh stiffnesses can be derived according to the following cases.

Case 1: When $h_{c1} \geq h_r$ & $\alpha_1 > \alpha_g$ [45]

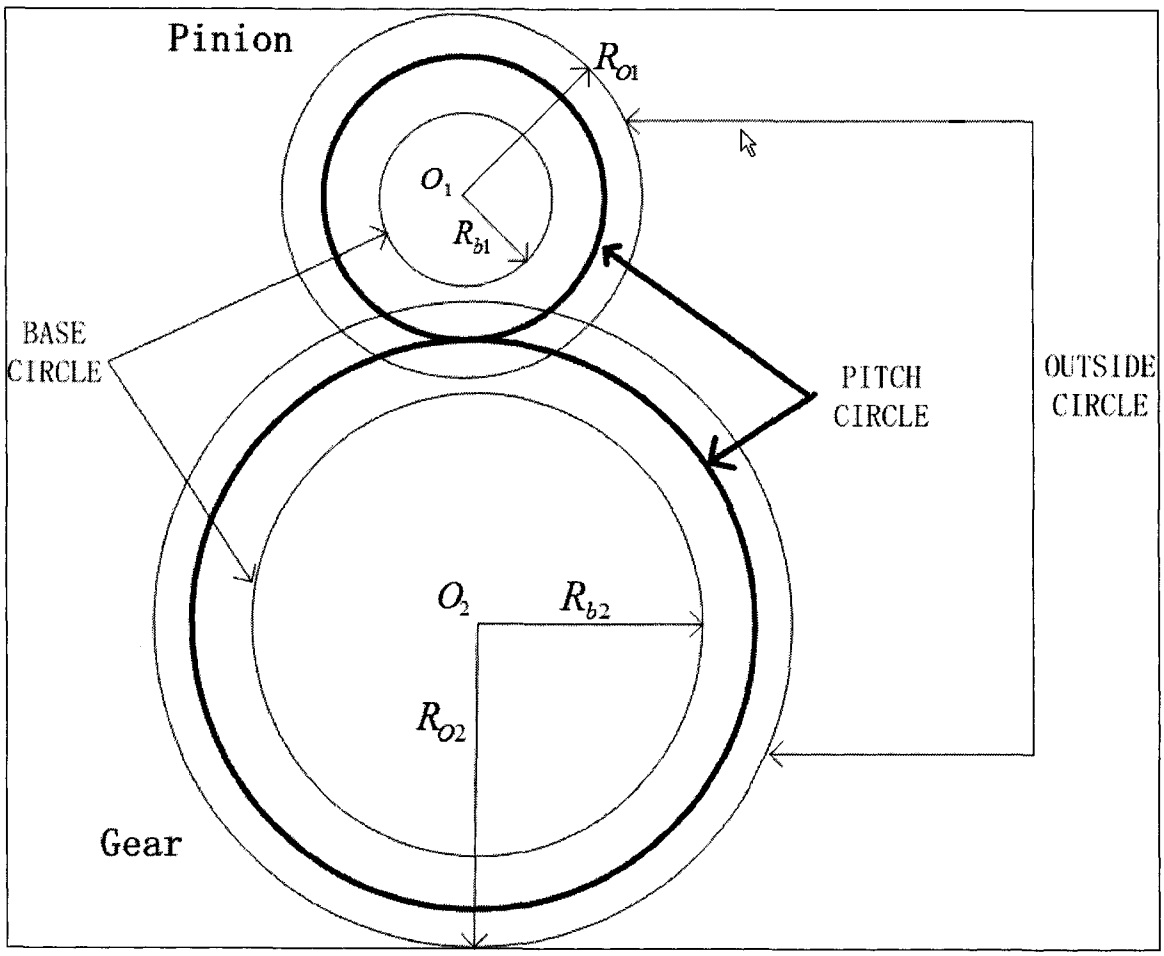

Figure 3.8: A two-dimensional pinion and gear

Referring to q_1 in Figure 3.7 and comparing that with the perfect gear tooth as shown in 3.1, when the crack first starts in the tooth's root, h_{c1} is larger than h_r, thus the effective area moment of inertia and area of cross section at a distance of x from the tooth's root can be calculated as Equations (3.34) and (3.35), respectively.

$$I_{xc} = \begin{cases} \frac{1}{12}(h_{c1} + h_x)^3 L, & \text{if } x \leq g_c \\ \frac{1}{12}(2h_x)^3 L, & \text{if } x > g_c \end{cases} \tag{3.34}$$

$$A_{xc} = \begin{cases} (h_{c1} + h_x)L, & \text{if } x \leq g_c \\ 2h_x L, & \text{if } x > g_c. \end{cases} \tag{3.35}$$

Replace the I_x and A_x in Equations (3.13) and (3.14) with I_{xc} and A_{xc}; after simplification, the bending mesh stiffness of the cracked tooth is:

$$\begin{aligned} \frac{1}{k_{b_{crack}}} &= \int_{-\alpha_g}^{\alpha_2} \frac{12\{1 + \cos\alpha_1[(\alpha_2 - \alpha)\sin\alpha - \cos\alpha]\}^2(\alpha_2 - \alpha)\cos\alpha}{EL[\sin\alpha_2 - \frac{q_1}{R_{b1}}\sin\upsilon + \sin\alpha + (\alpha_2 - \alpha)\cos\alpha]^3} \mathrm{d}\alpha \\ &+ \int_{-\alpha_1}^{-\alpha_g} \frac{3\{1 + \cos\alpha_1[(\alpha_2 - \alpha)\sin\alpha - \cos\alpha]\}^2(\alpha_2 - \alpha)\cos\alpha}{2EL[\sin\alpha + (\alpha_2 - \alpha)\cos\alpha]^3} \mathrm{d}\alpha \end{aligned} \tag{3.36}$$

and the shear mesh stiffness of the cracked tooth is:

$$\begin{aligned} \frac{1}{k_{s_{crack}}} &= \int_{-\alpha_g}^{\alpha_2} \frac{2.4(1+\nu)(\alpha_2 - \alpha)\cos\alpha(cos\alpha_1)^2}{EL[\sin\alpha_2 - \frac{q_1}{R_{b1}}\sin\upsilon + \sin\alpha + (\alpha_2 - \alpha)\cos\alpha]} \mathrm{d}\alpha \\ &+ \int_{-\alpha_1}^{-\alpha_g} \frac{1.2(1+\nu)(\alpha_2 - \alpha)\cos\alpha(\cos\alpha_1)^2}{EL[\sin\alpha + (\alpha_2 - \alpha)\cos\alpha]} \mathrm{d}\alpha. \end{aligned} \tag{3.37}$$

Case 2: When $h_{c1} < h_r$ or when $h_{c1} \geq h_r$ & $\alpha_1 \leq \alpha_g$ [45]

Referring to q_1 in Figure 3.9 and comparing that with the perfect gear tooth as shown in 3.1, in this case, the effective area moment of inertia and

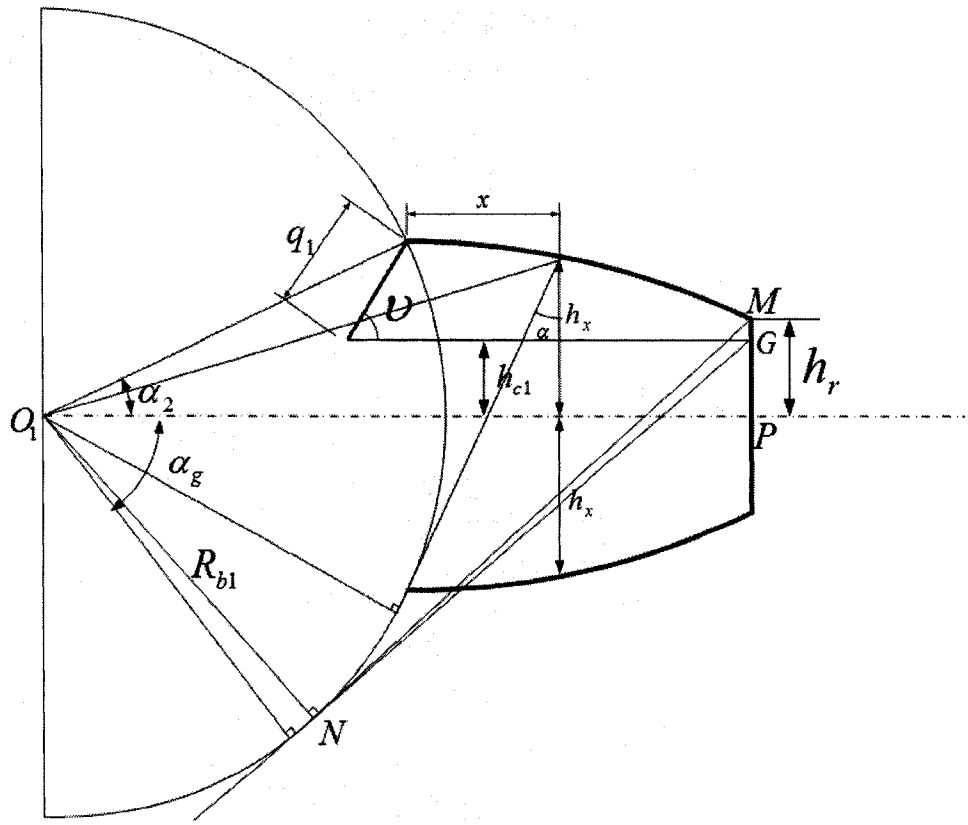

Figure 3.9: A cracked tooth model for **Case 2**

area of cross section at a distance of x from the tooth's root will be calculated as Equations (3.38) and (3.39), respectively.

$$I_{xc} = \frac{1}{12}(h_{c1} + h_x)^3 L \tag{3.38}$$

$$A_{xc} = (h_{c1} + h_x)L. \tag{3.39}$$

Then the bending mesh stiffness of the cracked tooth is:

$$\frac{1}{k_{b_{crack}}} = \int_{-\alpha_1}^{\alpha_2} \frac{12\{1 + \cos\alpha_1[(\alpha_2 - \alpha)\sin\alpha - \cos\alpha]\}^2(\alpha_2 - \alpha)\cos\alpha}{EL[\sin\alpha_2 - \frac{q_1'}{R_{b1}}\sin\upsilon + \sin\alpha + (\alpha_2 - \alpha)\cos\alpha]^3}\mathrm{d}\alpha \tag{3.40}$$

and the shear mesh stiffness of the cracked tooth is:

$$\frac{1}{k_{s_{crack}}} = \int_{-\alpha_1}^{\alpha_2} \frac{2.4(1+\nu)(\alpha_2 - \alpha)\cos\alpha(\cos\alpha_1)^2}{EL[\sin\alpha_2 - \frac{q_1'}{R_{b1}}\sin\upsilon + \sin\alpha + (\alpha_2 - \alpha)\cos\alpha]}\mathrm{d}\alpha. \tag{3.41}$$

The critical point between **Case 1** and **Case 2** can be obtained at $h_r = h_{c1}$; it is $q_1 = 2.36$mm, based on the gear parameters shown in Table 3.1.

As we assume in the last section, when the crack develops to the tooth's central line, q_1 reaches its maximum value, 3.9mm, which can be easily calculated by Equation (3.26). Then, as shown in Figure 3.10, the crack will change direction to q_2, which is assumed to be exactly symmetric with q_1. Hence, for a given crack length, q_2, h_{c2} can be calculated by:

$$h_{c2} = q_2 \sin\upsilon. \tag{3.42}$$

Similarly, the algorithm of bending and shear stiffnesses with crack q_2 is considered under the following two conditions.

Case 3: When $h_{c2} < h_r$ or when $h_{c2} \geq h_r$ & $\alpha_1 \leq \alpha_g$

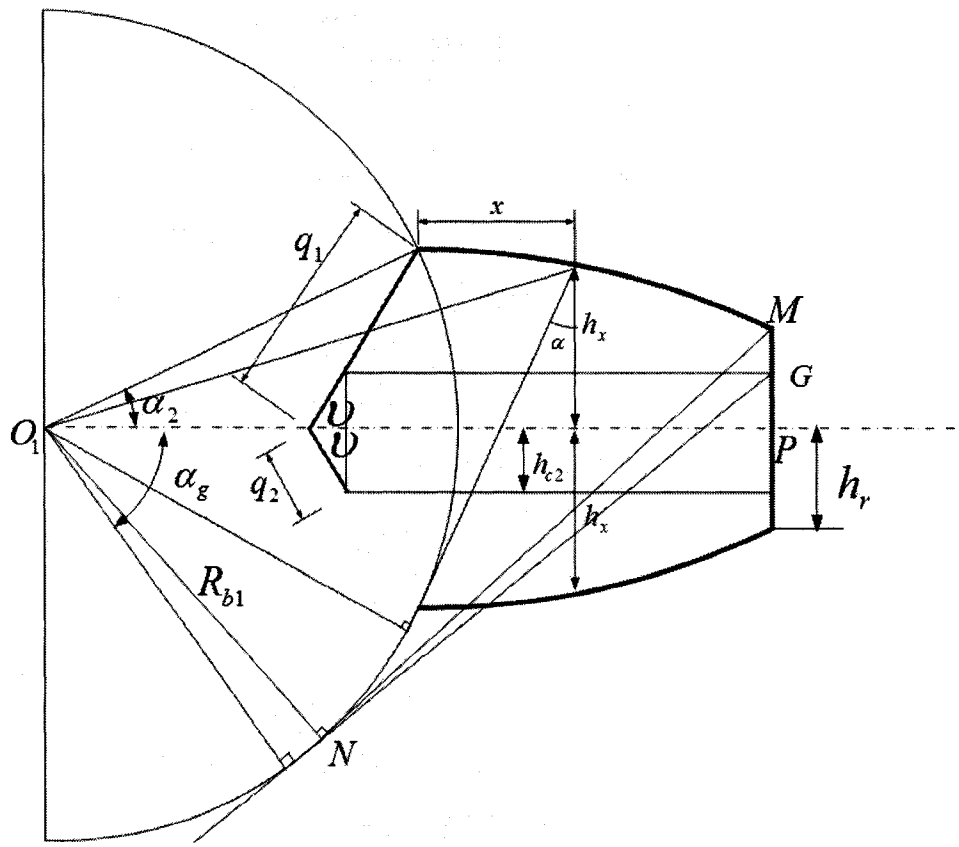

Figure 3.10: A cracked tooth model for **Case 3**

Referring to Equations (3.38) and (3.39) in **Case 2**, the effective area moment of inertia and area of cross section at a distance of x from the tooth root will be calculated as follows:

$$I_{xc} = \frac{1}{12}(h_x - h_{c2})^3 L = \frac{1}{12}(h_x - q_2 \sin \upsilon)^3 L \tag{3.43}$$

$$A_{xc} = (h_x - h_{c2})L = (h_x - q_2 sin\upsilon)L. \tag{3.44}$$

Then the bending mesh stiffness of the cracked tooth is:

$$\frac{1}{k_{b_{crack}}} = \int_{-\alpha_1}^{\alpha_2} \frac{12\{1+\cos\alpha_1[(\alpha_2-\alpha)\sin\alpha-\cos\alpha]\}^2(\alpha_2-\alpha)\cos\alpha}{EL[\sin\alpha+(\alpha_2-\alpha)\cos\alpha-\frac{q_2}{R_{b1}}\sin\upsilon]^3}\mathrm{d}\alpha \tag{3.45}$$

and the shear mesh stiffness of the cracked tooth is:

$$\frac{1}{k_{s_{crack}}} = \int_{-\alpha_1}^{\alpha_2} \frac{2.4(1+\nu)(\alpha_2-\alpha)\cos\alpha(\cos\alpha_1)^2}{EL[\sin\alpha+(\alpha_2-\alpha)\cos\alpha-\frac{q_2}{R_{b1}}\sin\upsilon]}\mathrm{d}\alpha. \tag{3.46}$$

Case 4: When $h_{c2} \geq h_r$ & $\alpha_1 > \alpha_g$

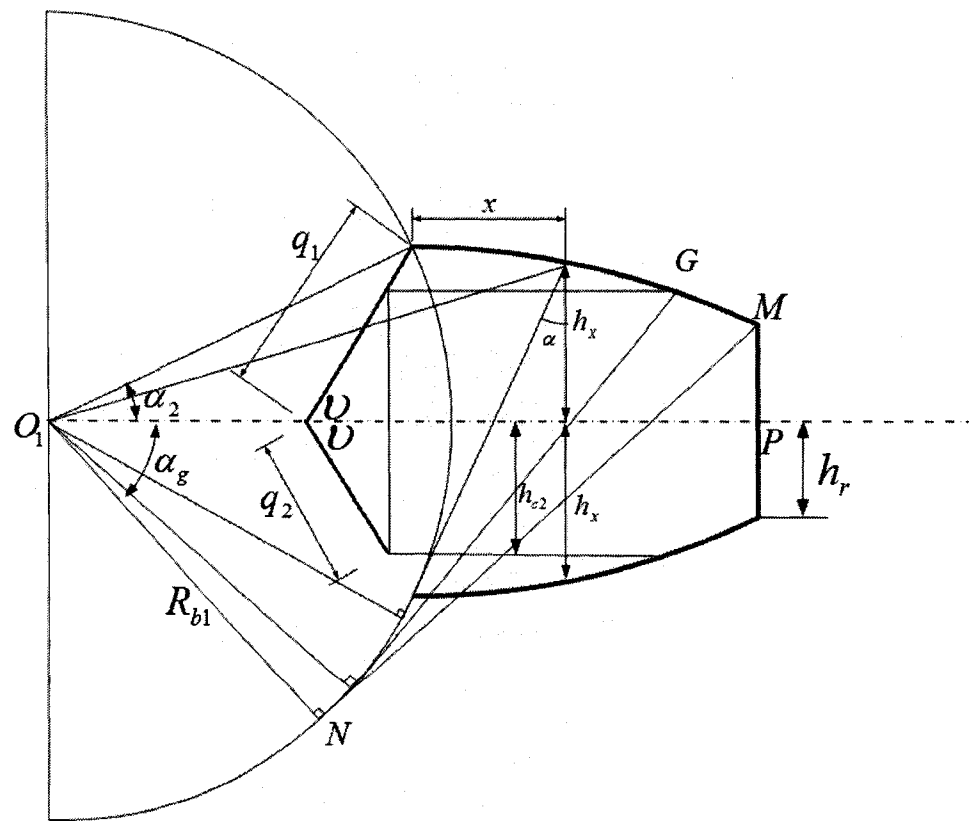

Figure 3.11: A cracked tooth model for **Case 4**

At the point $h_{c2} \geq h_x$, the mesh stiffness provided by this cross section is equal to zero. So we consider only the period in which $h_{c2} < h_x$. The equations of bending and shear mesh stiffness are similar to Equations (3.45) and (3.46).

Then the bending mesh stiffness of the cracked tooth is:

$$\frac{1}{k_{b_{crack}}} = \int_{-\alpha_g}^{\alpha_2} \frac{12\{1+\cos\alpha_1[(\alpha_2-\alpha)\sin\alpha-\cos\alpha]\}^2(\alpha_2-\alpha)\cos\alpha}{EL[\sin\alpha+(\alpha_2-\alpha)\cos\alpha-\frac{q_2}{R_{b1}}\sin\upsilon]^3}\mathrm{d}\alpha \quad (3.47)$$

and the shear mesh stiffness of the cracked tooth is:

$$\frac{1}{k_{s_{crack}}} = \int_{-\alpha_g}^{\alpha_2} \frac{2.4(1+\nu)(\alpha_2-\alpha)\cos\alpha(\cos\alpha_1)^2}{EL[\sin\alpha+(\alpha_2-\alpha)\cos\alpha-\frac{q_2}{R_{b1}}\sin\upsilon]}\mathrm{d}\alpha. \quad (3.48)$$

Again, the critical point between **Case 3** and **Case 4** can be obtained when $h_r = h_{c2}$; this is $q_2 = 1.54$mm, based on the gear parameters as shown in Table 3.1.

Thus, considering all four conditions, we can obtain the total effective mesh stiffness when only one pair of teeth are meshing and there exists a cracked tooth on the pinion.

$$k_{t_{crack}} = \frac{1}{\frac{1}{k_h}+\frac{1}{k_{b_{crack}}}+\frac{1}{k_{s_{crack}}}+\frac{1}{k_{a1}}+\frac{1}{k_{b2}}+\frac{1}{k_{s2}}+\frac{1}{k_{a2}}}. \quad (3.49)$$

Equation (3.49) is for the single-tooth-pair mesh period; when in the double-tooth-pair mesh period, the mesh stiffness provided by another pair of gear teeth must also be considered. Since the latter pair of teeth is in perfect condition, its mesh stiffness can be simply obtained through Equation (3.1). Then the total effective mesh stiffness in the double-tooth-pair mesh period is equal

to the sum of Equations (3.1) and (3.49).

Thus, for a pair of standard steel involute spur teeth whose main parameters are as shown in Table 3.1, consider a tooth's root crack as described in section 3.2, select the following crack length in Table 3.2, and their mesh stiffnesses can be calculated respectively.

Table 3.2: A sample of different crack lengths

$q_1 = 1.4$mm	**Case 1**
$q_1 = 3.1$mm	**Case 2**
$q_1 = 3.9$mm, $q_2 = 1.1$mm	**Case 3**
$q_1 = 3.9$mm, $q_2 = 2.4$mm	**Case 4**

Due to the influence of the tooth's root crack, with the deterioration of the crack levels, their total mesh stiffnesses drop greatly, and the calculation results are as shown in Figure 3.12.

So far, the procedure to obtain the analytical mesh stiffness model of a cracked spur gear tooth has been illustrated. From Figure 3.12, it can be observed that the presence of a crack in a tooth results in a local reduction of the mesh stiffness during one shaft rotation period. This is important information for future fault diagnosis. In Chapter 4, the dynamic model of gearbox system response will be established, and the total mesh stiffness of the gears will be substituted into a lumped parameter model to simulate the vibration response of gears under different deterioration levels of tooth crack.

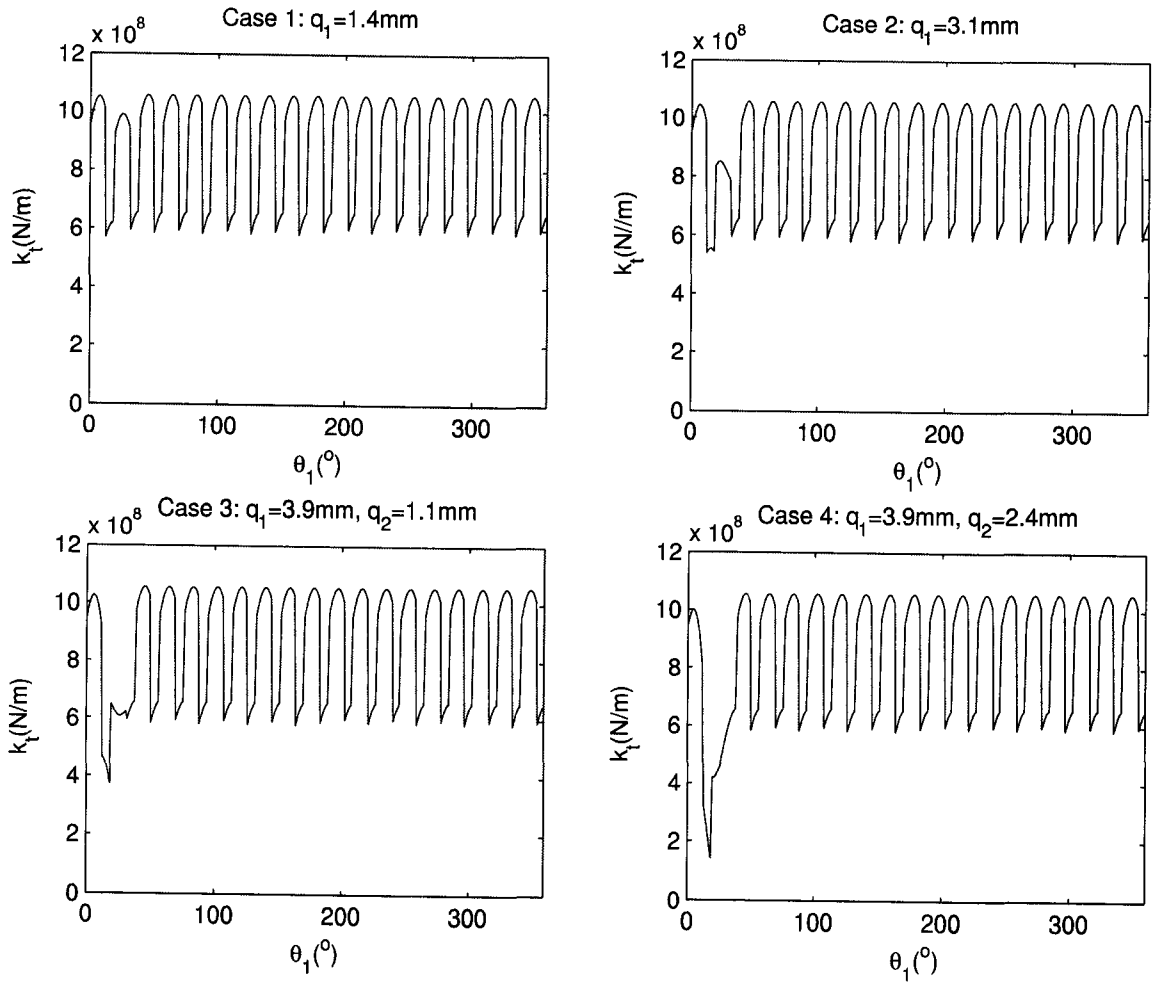

Figure 3.12: The total mesh stiffness, k_t, at different crack levels

Chapter 4

Dynamic Simulation of Gearbox System Responses

Since the tooth root crack model has been established, and the tooth mesh stiffness with or without the crack has been obtained, in this chapter, we will study the effect of the propagating fatigue crack on the gearbox vibration responses.

4.1 A Mathematical Model of Gearbox Vibration

A mathematical model with torsional and lateral vibration was described by Bartelmus [4] in 2001. The model of a one stage gearbox system is given in Figure 4.1. It is a two-parameter (stiffness and damping) model with torsional and lateral vibration, which means it includes both the linear and rotational equations of the system's motion. This model represents a system with six degrees of freedom, which is driven by electric motor moment, M_1, and is loaded with external moment, M_2. Inter-tooth friction is ignored here for simplicity's sake.

The following notations are used in this chapter:

- F_k: stiffness inter-tooth force

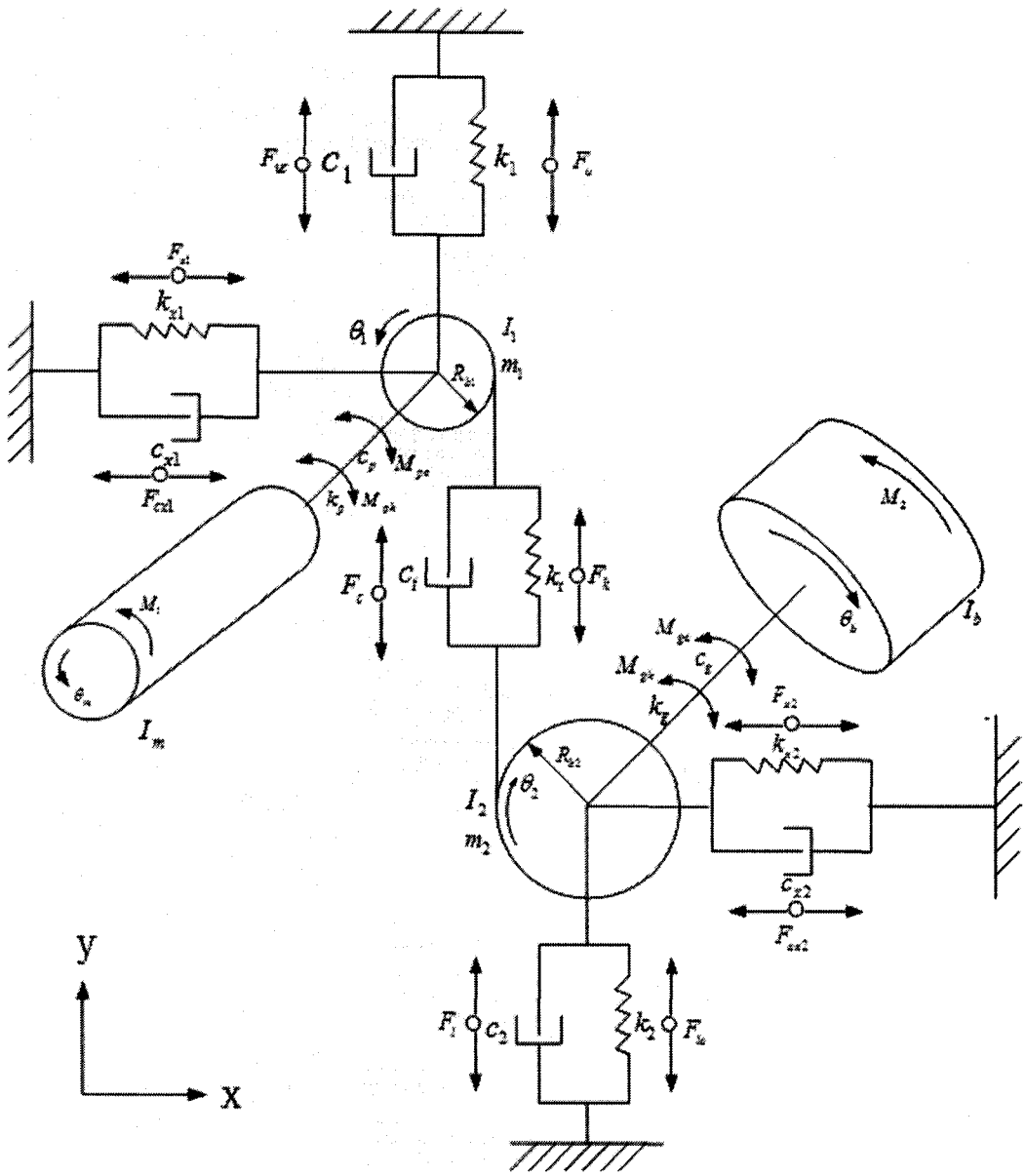

Figure 4.1: A one stage gearbox system [4]

- F_c: damping inter-tooth force
- F_u: internal stiffness force of input bearing
- F_{uc}: internal damping force of input bearing
- F_l: internal stiffness force of output bearing
- F_{lc}: internal damping force of output bearing
- M_{pk}: stiffness moment of input couplings
- M_{pc}: damping moment of input couplings
- M_{gk}: stiffness moment of output couplings
- M_{gc}: damping moment of output couplings
- k_t: total mesh stiffness
- c_t: mesh damping coefficient
- I_m: mass moment of inertia of motor
- I_b: mass moment of inertia of load
- I_1: mass moment of inertia of pinion
- I_2: mass moment of inertia of gear
- M_1: input motor torque
- M_2: output torque from load
- m_1: mass of the pinion
- m_2: mass of the gear
- R_{b1}: base circle radius of pinion
- R_{b2}: base circle radius of gear
- R_{O1}: outside circle radius of pinion

- R_{O2}: outside circle radius of gear
- k_p: torsional stiffness of input flexible coupling
- k_g: torsional stiffness of output flexible coupling
- c_p: damping coefficient of input flexible coupling
- c_g: damping coefficient of output flexible coupling
- k_1: vertical radial stiffness of input bearings
- k_2: vertical radial stiffness of output bearings
- c_1: vertical radial viscous damping coefficient of input bearings
- c_2: vertical radial viscous damping coefficient of output bearings
- y_1: linear displacement of pinion in the y direction
- y_2: linear displacement of gear in the y direction
- θ_m: angular displacement of motor
- θ_b: angular displacement of load
- θ_1: angular displacement of pinion
- θ_2: angular displacement of gear

According to [45], the vibration in x direction as shown in Figure 4.2 is free response and will disappear due to inherent damping, therefore we focus only on the motion in the y direction.

The equations of motion for the system take the forms that follow [4].

The vertical motion (in y direction) equations of the pinion and gear are:

$$\begin{aligned} m_1\ddot{y}_1 &= F_k + F_c - F_u - F_{uc} \\ m_2\ddot{y}_2 &= F_k + F_c - F_l - F_{lc}. \end{aligned} \tag{4.1}$$

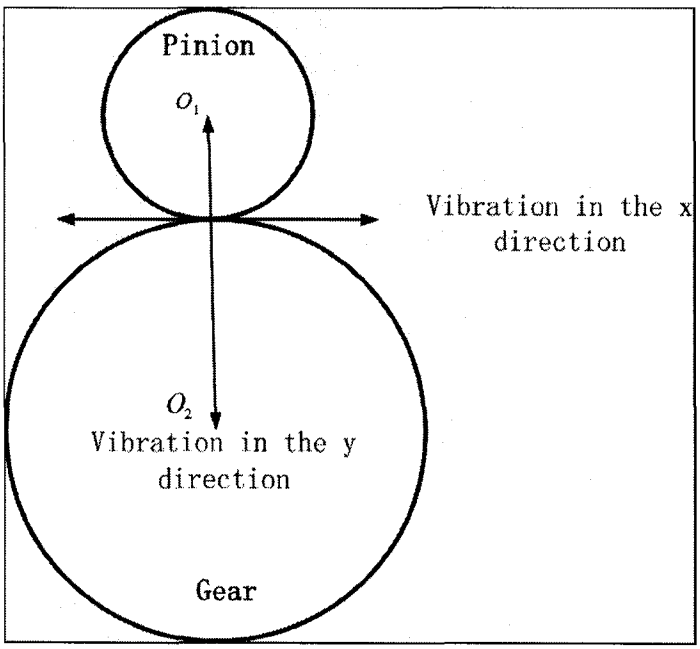

Figure 4.2: Indication of the vibration in the x and y directions

The rotary motion equations of the pinion and gear are:

$$\begin{aligned} I_1\ddot{\theta}_1 &= M_{pk} + M_{pc} - R_{b1}(F_k + F_c) \\ I_2\ddot{\theta}_2 &= R_{b2}(F_k + F_c) - M_{gk} - M_{gc}. \end{aligned} \tag{4.2}$$

The rotary motion equations of the motor and load are:

$$\begin{aligned} I_m\ddot{\theta}_m &= M_1 - M_{pk} - M_{pc} \\ I_b\ddot{\theta}_b &= -M_2 + M_{gk} + M_{gc}. \end{aligned} \tag{4.3}$$

The values of forces and moments are given by:

$$F_k = k_t(R_{b1}\theta_1 - R_{b2}\theta_2 - y_1 + y_2)$$

$$F_c = c_t(R_{b1}\dot{\theta}_1 - R_{b2}\dot{\theta}_2 - \dot{y}_1 + \dot{y}_2) \tag{4.4}$$

$$\begin{aligned} F_u &= k_1 y_1 \\ F_{uc} &= c_1 \dot{y}_1 \\ F_l &= k_2 y_2 \\ F_{lc} &= c_2 \dot{y}_2 \end{aligned} \tag{4.5}$$

$$\begin{aligned} M_{pk} &= k_p(\theta_m - \theta_1) \\ M_{pc} &= c_p(\dot{\theta_m} - \dot{\theta}_1) \\ M_{gk} &= k_g(\theta_2 - \theta_b) \\ M_{gc} &= c_g(\dot{\theta}_2 - \dot{\theta}_b). \end{aligned} \tag{4.6}$$

Equation (4.1) indicates that periodic time varying mesh stiffness is the main source of the gear vibration. Since the model has been established, the next step is to use these sets of equations for computer simulation when the gear is new or cracked.

4.2 Computer Simulation for Perfect Gears

For the purpose of inferring damages from vibration data, the perfect gear's vibration signal is a necessary reference. According to the simplified conditions described in [45], the vertical radial stiffness of the input bearings, k_1, and output bearings, k_2, are assumed to be a constant k_r; the damping coefficient

of the input bearings, c_1, and output bearings, c_2, are assumed to have a constant c_r; the torsional stiffness of the input flexible coupling, k_p, and the output flexible coupling, k_g, are equal to k_c; the damping coefficient of the input flexible coupling, c_p, and the output flexible coupling, c_g, are equal to c_c. Also, the mesh damping coefficient, c_t, is set to be proportional to the total mesh stiffness, k_t, which is [45]:

$$c_t = \mu k_t \tag{4.7}$$

where μ is the scale constant with units of second, and its value has been selected in this simulation as $3.99 \times 10^{-6}(s)$. Furthermore, the other parameters of the gearbox system are listed in Table 4.1.

Table 4.1: Main parameters of the gearbox system [45]

Mass of the pinion	$m_1 = 0.96kg$
Mass of the gear	$m_2 = 2.88kg$
Contact ratio	$C_r = 1.6456$
Mass moment of inertia of the motor	$I_m = 0.0021kgm^2$
Mass moment of inertia of the load	$I_b = 0.0105kgm^2$
Mass moment of inertia of the pinion	$I_1 = 4.3659 \times 10^{-4}kgm^2$
Mass moment of inertia of the gear	$I_2 = 8.3602 \times 10^{-3}kgm^2$
Input shaft frequency	$f_1 = 30Hz$
Mesh frequency	$f_m = 570Hz$
Input motor torque	$M_1 = 11.9Nm$
Output load torque	$M_2 = 48.8Nm$
Torsional stiffness of the coupling	$k_c = 4.4 \times 10^4 Nm/rad$
Damping coefficient of the coupling	$c_c = 5.0 \times 10^5 Nm/rad$
Radial stiffness of the bearing	$k_r = 6.56 \times 10^7 N/m$
Damping coefficient of the bearing	$c_r = 1.8 \times 10^5 Ns/m$

Given the above, we simply need to apply these parameters and the time varying mesh stiffness to Equations (4.1) - (4.3). Based on Chapter 3, the numerical values for the total mesh stiffness, k_t, when the gears are in perfect

condition have been obtained, and are as shown in Figure 3.2. In order to make the values in Figure 3.2 applicable, a simpler function is required to express the relationship between k_t and time t. From the work of Li et al.[29], a truncated Fourier series with a fundamental frequency of tooth meshing can be used to represent the k_t of a good gear.

$$k_g(t) = \frac{a_0}{2} + \sum_{r=1}^{R}(a_r \cos(2\pi r f_m t) + b_r \sin(2\pi r f_m t)) \tag{4.8}$$

where R is the number of harmonics included, and f_m is the meshing frequency.

In Equation (4.8), f_m is the known parameter, which according to Table 4.1 is 570Hz. Then, MATLAB's LSQCURVEFIT function is used to obtain the parameters a_r and b_r based on the known values for time, t, and mesh stiffness, k_t. Generally, the larger the number of harmonics, R, the higher the curvefit accuracy; but the complexity of the expression increases, becoming time-consuming and inconvenient to use in the motion equations. By trading off these factors, R is set at 40 and the numerical values for a_r and b_r can be automatically derived through the MATLAB program. Thus, insert a_1 to a_{40} and b_1 to b_{40} into Equation (4.8) and the mesh stiffness, k_t, can be expressed as a function of time, $t(s)$. See plot (b) in Figure 4.3.

Then, plot the numerical values of the mesh stiffness, k_t, in (a), by comparing plots (a) and (b). It is observed that their difference is very small. Since the computer simulation itself is an approximation process based on many simplifications, small errors can be ignored. Thus, we believe that using Equation (4.8) to represent the mesh stiffness, k_t, with time, t, is successful.

So far, all the parameters required in the dynamic models have been determined; however, due to the complexity of the differential Equations (4.1) - (4.3), the analytical solutions cannot be derived. The alternative is to find

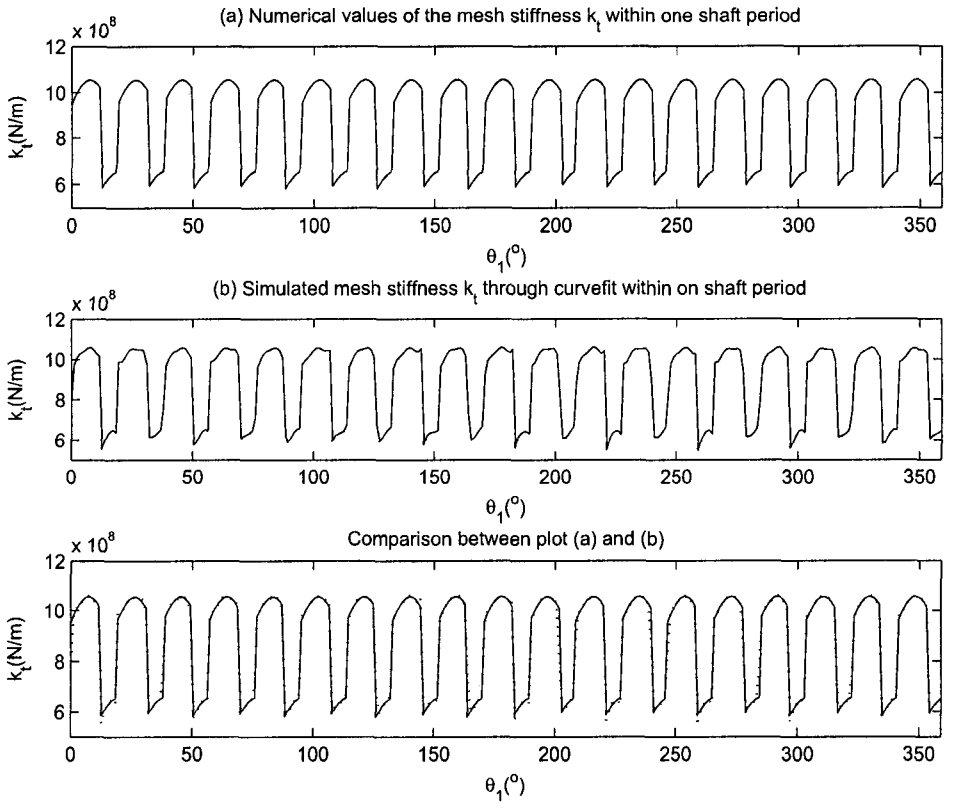

Figure 4.3: The comparison between the numerical values of k_t and their simulation values through curvefit

their numerical solutions by means of MATLAB.

MATLAB's ODE15s is a standard solver in MATLAB for ordinary differential equations. The Runge-Kutta method is implemented in this function. Thus, in this study, the function of ODE15s is used to obtain the numerical results of the motion equations. The integration step size Δt used here is equal to 0.0001s by considering the necessary calculation accuracy, without taking too much computation time.

Then, the displacement plots for the perfect gear tooth can be obtained by computer simulations; and the results are presented in Figure 4.4.

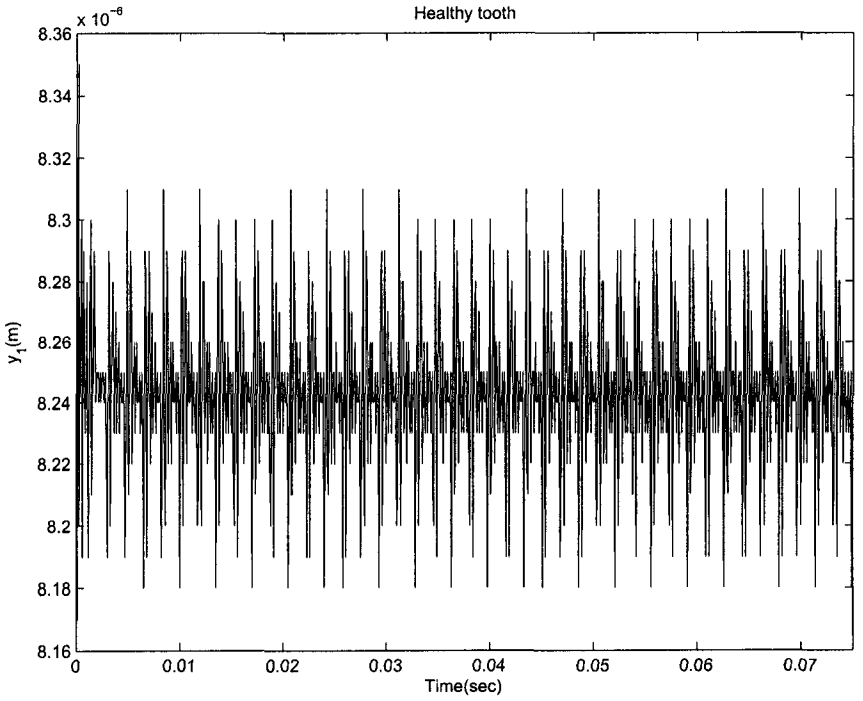

Figure 4.4: The pinion's vibration displacement response in the y direction for a perfect gear tooth

Figure 4.4 shows the pinion's vibration response in more than two shaft rotation periods (t = 0.0725s) when one shaft rotation period is equal to

$1/f_1 = 1/30\text{Hz} = 0.0333\text{s}$. Ideally, the meshing vibrations in each meshing period should be exactly the same because, for perfect gears, the meshing condition of each gear tooth is identical; however, in Figure 4.4, the meshing vibrations are not exactly the same in each meshing period. The reason is that we are trying to use a simple function to express the relationship between k_t and time, t, therefore we have used the curvefit method to simulate the mesh stiffness, k_t, in Equation (4.8). Since this is an approximate process, errors must arise during the simulation; these errors cause the above phenomenon.

In order to observe more details, the Fourier Transform is applied to the time domain signal, and the power spectral density is presented in Figure 4.5.

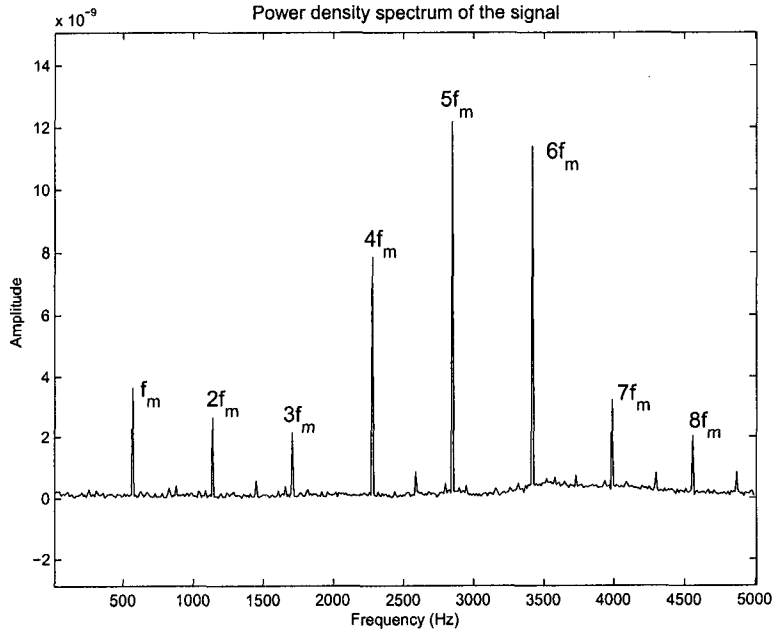

Figure 4.5: Spectra of the pinion's vibration displacement response in the y direction for a perfect gear tooth

As shown in Figure 4.5, for the perfect gear tooth, the spectrum of the vibration signal is very clear; only the mesh frequency ($f_m = 570\text{Hz}$) and its

harmonic components dominate the signal. This matches our expectation of the perfect gear vibration signal, thus, we believe the errors caused by approximating the expression of the mesh stiffness does not greatly affect the simulation results. Moreover, among those harmonics, it is found that the fourth, fifth and sixth harmonics of the tooth meshing frequency are the most dominant spectral components. For this reason, the time domain and frequency domain signal of the perfect gear tooth can be considered the reference signal, and can be compared with the cracked gear tooth vibration signal in analyses to come.

4.3 Computer Simulation for a Pinion with a Cracked Tooth

This section will focus on the dynamic response of fatigue cracks. Since a damaged tooth suffers a larger deflection than a perfect one, it will undergo an appropriate reduction in time-varying mesh stiffness that is repeated only once in a revolution. As a result, a Fourier series with a fundamental frequency as the rotation frequency is used according to [29].

$$k_g(t) = (1+\sum_{l=1}^{L}[c_l \cos(2\pi l f_s t)+d_l \sin(2\pi l f_s t)])(\frac{a_0}{2}+\sum_{r=1}^{R}[a_n \cos(2\pi r f_m t)+b_n \sin(2\pi r f_m t)]) \tag{4.9}$$

where L is the number of harmonics considered and f_s is the gear rotating frequency, which in this thesis is equal to f_1. Thus, it is obvious that Equation (4.8) is a special case of Equation (4.9). For the healthy gear pair, the meshing stiffnesses of each tooth are almost identical. On the other hand, for the faulty gear pair, the additional term, L, is included to express the meshing pattern that appears only once in a shaft revolution.

In the same way the perfect gear vibration signal is simulated, based on the known values of time, t, and the time-varying mesh stiffness, k_t. MATLAB's LSQCURVEFIT function is still used to obtain the parameters a_n, b_n, c_l and d_l in Equation (4.9). By considering both curvefit accuracy and computer processing time, the number of harmonics, N and L, is set at 40 and 80 respectively. This done, the parameters a_1 to a_{40}, b_1 to b_{40}, c_1 to c_{80} and d_1 to d_{80} can all be simulated and used to express the relationship between $k_g(t)$ and time, t, in Equation (4.9).

To validate the above procedure, we set the crack level at 0% and use Equation (4.9) to calculate the mesh stiffness. Compared to the perfect gear mesh stiffness derived from Equation (4.8), Figure 4.6, shows clearly that these two simulation results are nearly the same.

After all, still by means of MATLAB's ODE15s function, the displacement plots can be derived for the cracked gear tooth with increasing deterioration levels. As described before, the initial crack length is set at 0.1mm, and the increment size is also 0.1mm. Up to the point of total tooth breakage, the full crack length is 7.8mm. To make the severity of the fault clearer, the percentage between the current crack length and the full crack length is used to represent the current crack level. Thus, the initial crack is around 1% and the increment size is approximately 1% to 2%. Since the tooth may suffer a sudden breakage before the crack develops to its full length, the maximum crack level is assumed to be 80%. Figures 4.7 and 4.8 show some examples of cracked tooth dynamic responses.

In Figure 4.7, the fault influences are not very obvious to visual observation; the signals look very similar compared to the perfect gear vibration signal shown in Figure 4.4. It is clear, however, the appearance of the tooth root

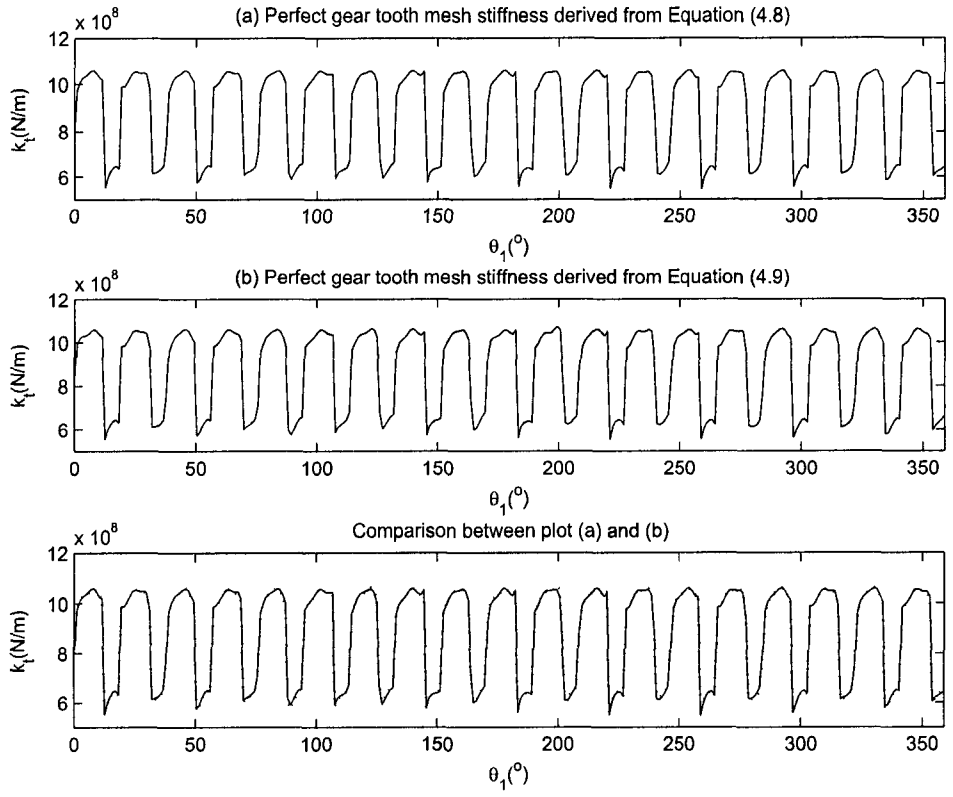

Figure 4.6: Comparison of the perfect gear tooth mesh stiffness derived from Equations (4.8) and (4.9)

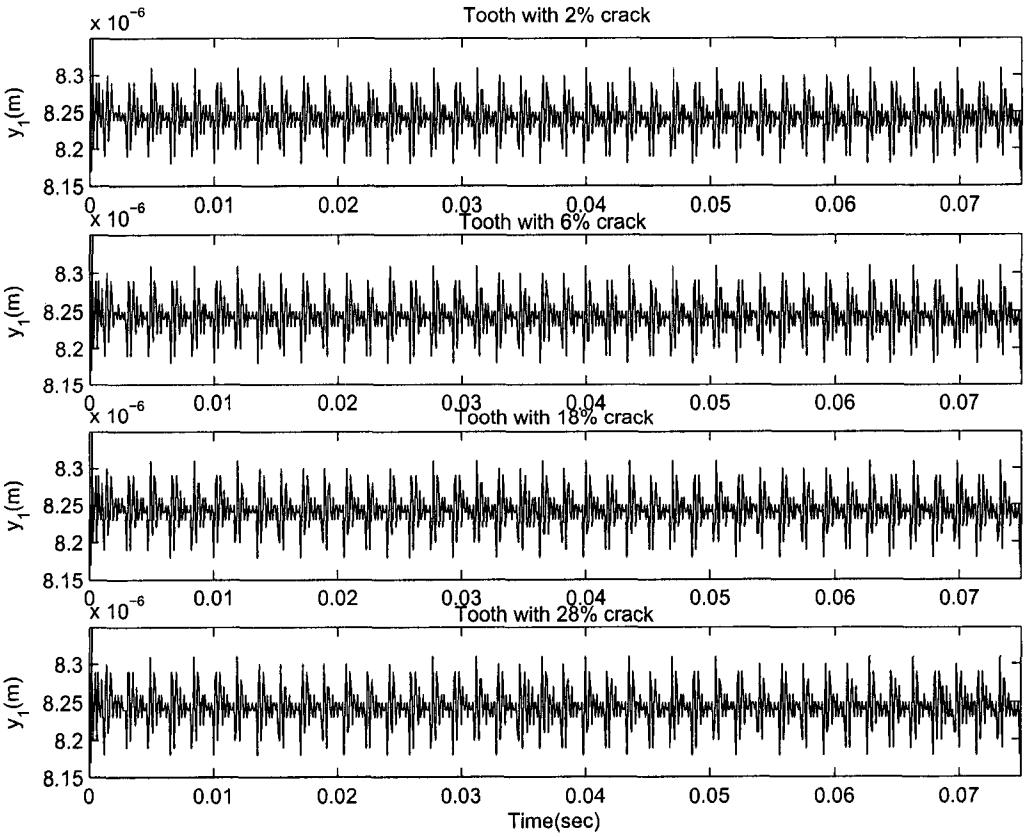

Figure 4.7: The pinion's vibration displacement response in the y direction for a cracked gear tooth

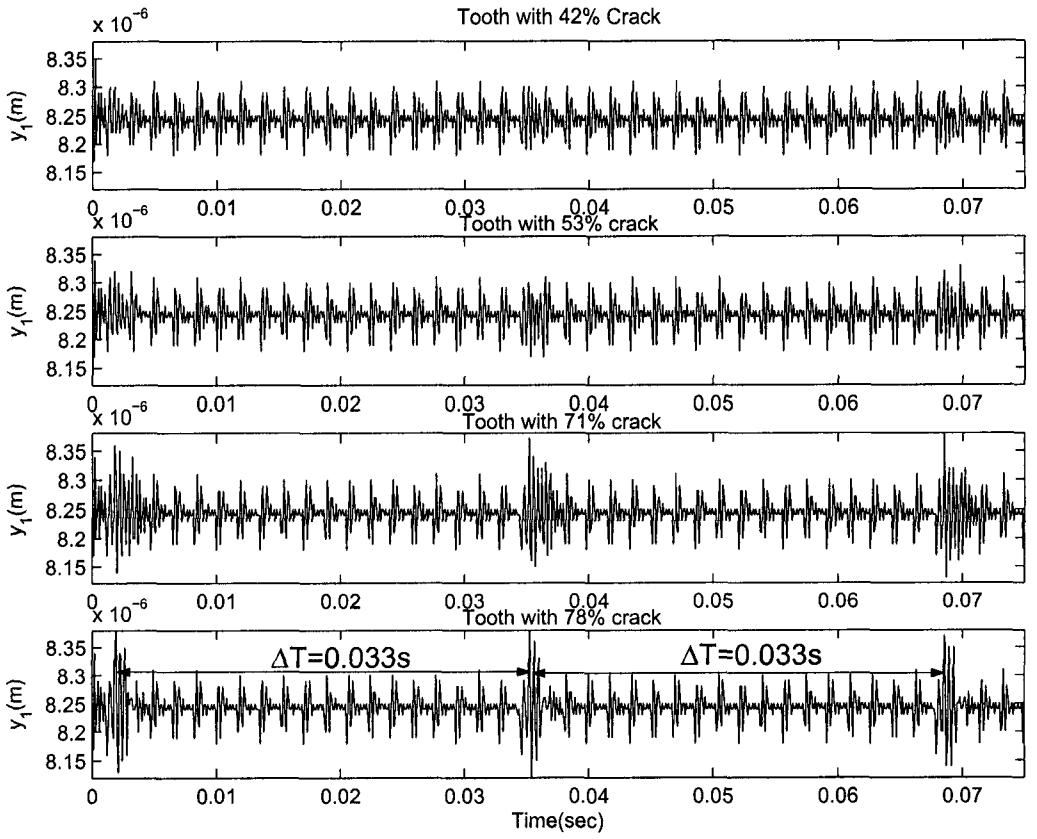

Figure 4.8: The pinion's vibration displacement response in the y direction for a cracked gear tooth

crack produces changes in the gear vibration signals in Figure 4.8. The obvious periodical impulses caused by the mating tooth appear in the time domain signal as the crack level increases; this carries diagnostic information that is important for extracting features of tooth defects. Because the influence caused by the cracked tooth repeats only once in a revolution, the duration between every two impulses is equal to one shaft period ($T_1 = 1/f_1 = 0.033s$). For comparison with the perfect gear vibration signal, the Fourier Transform is applied to the cracked gear tooth vibration signal, and some examples of the power spectral density plots are presented in Figures 4.9 and 4.10.

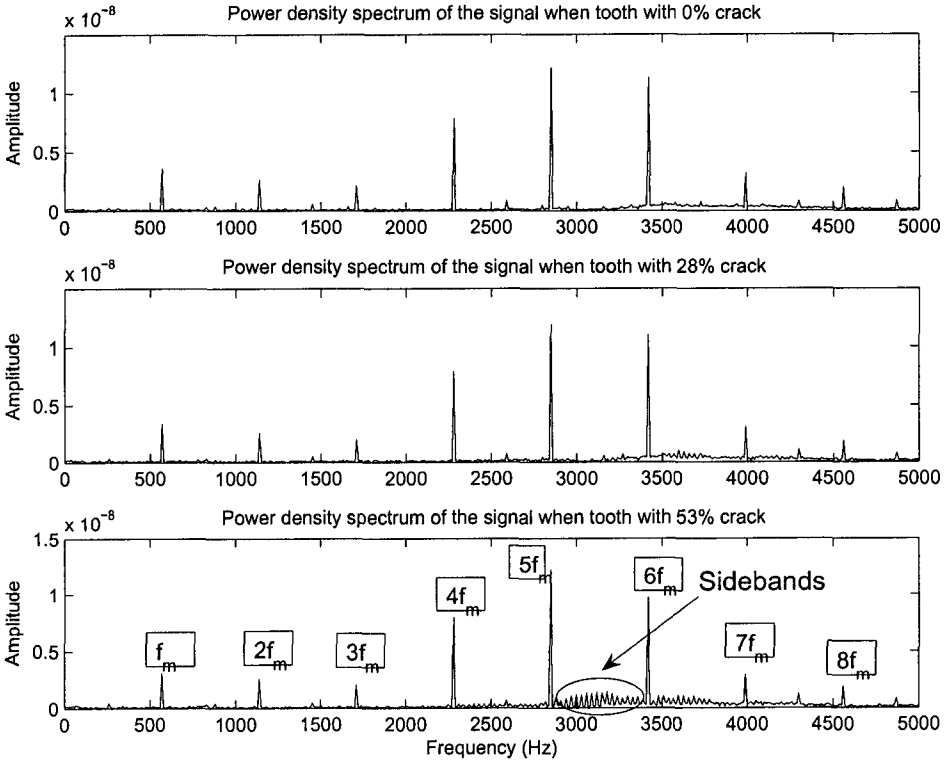

Figure 4.9: Spectra of a pinion's vibration displacement response in the y direction for a cracked gear tooth

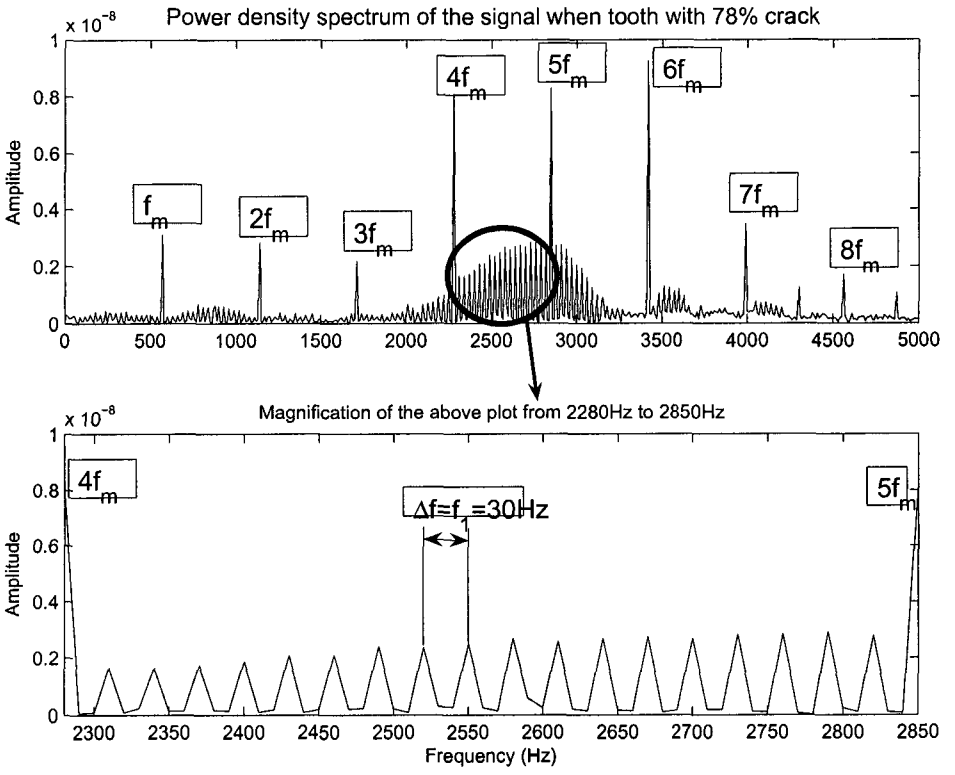

Figure 4.10: Spectra of a pinion's vibration displacement response in the y direction for a tooth with a 78% crack

As shown in Figure 4.9, when the crack level is 28%, the frequency spectrum is still very clear, no obvious difference can be detected compared to the perfect gear spectrum shown in Figure 4.5; however, as the crack increases to 53%, sidebands start to appear between the fifth and sixth meshing frequency harmonics ($5f_m$ and $6f_m$). In Figure 4.10, since the crack reaches 78%, the modulation sidebands become very significant. These sidebands are located on both sides of the gear tooth meshing frequency ($f_m = 570$Hz) and its harmonics, especially between the fourth and fifth mesh frequency harmonics. After magnifying the plot between $4f_m$ and $5f_m$, it can easily be determined that the distance between every two adjacent sidebands is exactly equal to the input shaft frequency ($f_1 = 30Hz$). Thus, the faults in the gearbox system are strongly indicated by clear patterns of sidebands around the meshing frequency harmonics.

From the above discussion, we concluded that the modifications of the vibration signals caused by the initiation of the tooth crack can hardly be detected through visual observation. The dynamic response in the time domain remains constant; as long as the perfect gear pair and its frequency spectrum are clear, only the meshing frequency and its harmonics are dominant. As the crack propagates to the medium and severe levels, the fault is gradually indicated by a transient impulse in the time domain and a cluster of sidebands around the meshing frequency harmonics. These faulty features appear too late, however, for our early fault detection purpose. In Chapter 5, several statistical techniques will be applied to simulated vibration signals in order to demonstrate the use of a scientific method of giving an early warning of tooth damage. In addition, a useful condition indicator will be extracted to reflect fault initiation and deterioration.

CHAPTER 5

DEGRADATION ESTIMATION USING STATISTICAL TECHNIQUES

Since a number of vibration signals of perfect and cracked gear teeth have been simulated, the purpose of this chapter is to try different statistical techniques in order to find a simple but effective way of providing a warning of damage early enough to avoid sudden tooth breakage. The methods of vibration analysis in use in this thesis include time-domain analysis and frequency domain analysis.

5.1 Time Domain Indices Applied to Original Signals

Time-domain analysis is the most fundamental and easily implemented method of vibration analysis. Since the presence of a tooth crack leads to a reduction in total mesh stiffness, this will require a minor or significant modification of the dynamic response. As described in Chapter 4, Figures 4.7 and 4.8 represent the vibration signal with increasing crack levels. Distinct impulses can be detected by visual observation when a crack reaches 70%. In contrast, for the initial or medium crack, though we believe it must cause modifications to the vibration signal, no damage features can be easily identified through visual observation. The most general approach is to select a proper indicator to extract defect

features from the vibration signal and then track the fault evolution in the equipment.

A number of simple signal metrics based on the time domain waveform still have widespread application in mechanical fault detection, the simplest of these being the RMS (Root Mean Square) value of the signal which is used for overall vibration level measurements [16]. RMS is a kind of average of the signal; for discrete signals, the RMS value is defined as [16]:

$$\begin{aligned} \text{RMS} &= \sqrt{\frac{1}{N}\sum_{n=1}^{N}(x(n)-\bar{x})^2} \\ \bar{x} &= \frac{1}{N}\sum_{n=1}^{N}x(n) \end{aligned} \tag{5.1}$$

where N is the number of samples taken in the signal, $x(n)$ is the amplitude of the signal for the nth sample, and $\bar{x}$ is the mean value of all the amplitudes. RMS is one of the most conventional statistical indices, and it is very simply conducted for machine condition-monitoring applications. However, since RMS is a method that indicates the trend of the overall vibration level, it is not sensitive to impulses in the signal until they increase significantly.

As described in Chapter 2, in the past few years, higher order statistics has been garnering more intensive interest, and kurtosis is the most basic statistical tool. Kurtosis is a parameter that is sensitive to the shape of the signal and is well adapted to the impulse nature of the stimulating forces generated by component damage [9]. Its value can be given by [9]:

$$\text{kurtosis} = \frac{\frac{1}{N}\sum_{n=1}^{N}(x(n)-\bar{x})^4}{[\frac{1}{N}\sum_{n=1}^{N}(x(n)-\bar{x})^2]^2}. \tag{5.2}$$

Similar to kurtosis, a third statistical moment parameter, S_r, was developed in [20]. It has been found to have the same traditional merit as kurtosis, and it is less sensitive to spurious vibrations and more stable under different loads and speeds. The equation for S_r is given as follows [44]:

$$S_r = \frac{\frac{1}{N}\sum_{n=1}^{N}[(x(n)-\bar{x})^2]^{3/2}}{[\frac{1}{N}\sum_{n=1}^{N}(x(n)-\bar{x})^2]^{3/2}}. \tag{5.3}$$

Based on the findings of [44], kurtosis and S_r are the two major diagnostic indices in statistical moment analysis; however, both kurtosis and S_r have their own advantages and disadvantages. Thus, a new statistical moment, S_α was developed in [44]; it has lower susceptibility to spurious vibrations than kurtosis and higher sensitivity to impulse signals than S_r. It is defined as [44]:

$$S_\alpha = \frac{\frac{1}{N}\sum_{n=1}^{N}|x(n)-\bar{x}|^3}{(\frac{1}{N}\sum_{n=1}^{N}|x(n)-\bar{x}|)^3}. \tag{5.4}$$

FGP (Fault Growth Parameter) is another new indicator that has been reviewed in detail in Chapter 2; its revised version is FGP1. Their algorithm are shown in Equations (2.5) and (2.6).

In this chapter, we will calculate the following indicators: S_α, S_r, RMS, kurtosis, FGP and FGP1; each has its own unique features useful in fault diagnosis, and each is based on numerically simulated vibration signals obtained from Chapter 4. These indicators are valuable tools in the search for the most effective way of detecting equipment faults in the early stages and tracking deterioration scientifically.

In keeping with Chapter 3, the type of fault considered here is a root crack on a tooth of the pinion, varying from 1% to 80%, and with increments of approximately 1%. For each crack level, a group of vibration displacements

can be simulated; these have already been illustrated in Figures 4.7 and 4.8. For comparison, a perfect gear signal has also been simulated in Figure 4.4 as a reference signal. For each gear condition, the total number of data points in the time domain is $N = 1000$ and the amplitude of each data point is $x(n)$. The time period is from 0 to 0.1s; since one shaft revolution is 0.03s, the vibration signal contains approximately 3.33 revolutions in total. Then, the values of S_α, S_r, RMS, kurtosis, FGP and FGP1 can be calculated for each tooth condition. Our purpose is to find an effective way to compare these calculation results in the same scale. Since the values of FGP and FGP1 represent the outlier percentage of cracked tooth vibration compared to the healthy tooth vibration signal, and the other indicators only show the actual values of the cracked tooth vibration signals; to make them comparable, we want to make all the indicators represent changes from the healthy condition. Let's use kurtosis as an example. We deduct the healthy tooth kurtosis from the cracked one, divide the difference by the healthy tooth kurtosis, and express the result in the form of percentage. This value shows the change of cracked tooth kurtosis from the healthy one. Repeat the same procedure for RMS, S_α and S_r, and the calculation results are shown in Figure 5.1.

It can be observed that the values for FGP and FGP1 remain almost the same during the whole process. Their trends develop along an almost horizontal straight line, and at the same time, the values of RMS fluctuated around the x axes. Neither of these two indicators provide useful characteristics that can be used to reveal the deterioration of the tooth crack.

As to kurtosis and S_α, they have a very similar increasing trend. Until the crack reaches 60%, their values remain pretty constant with slight increases. Then, from 60% to 80%, the crack's influence begins to disturb the vibration

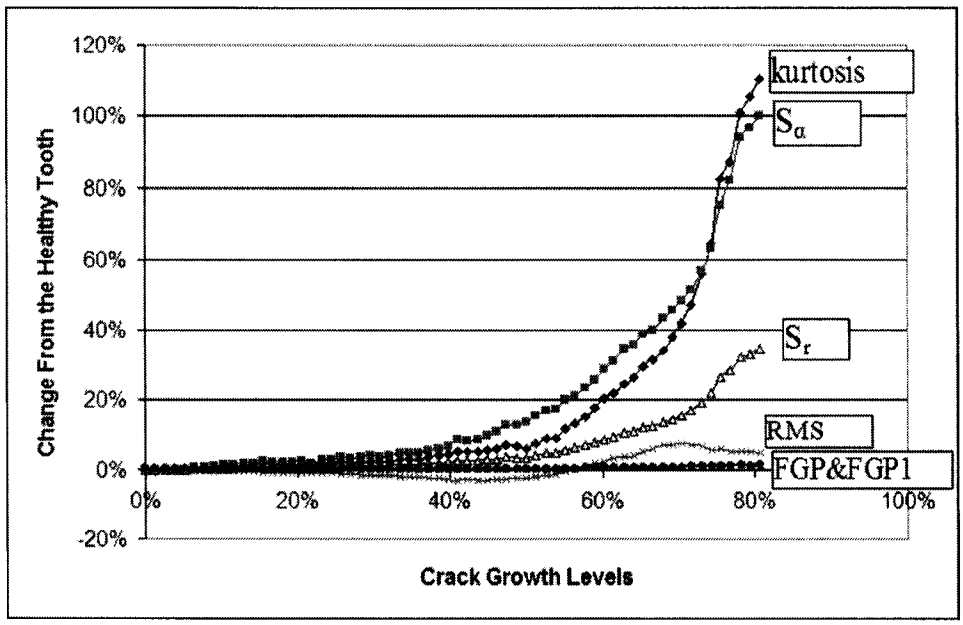

Figure 5.1: Comparison among S_α, S_r, kurtosis, RMS, FGP and FGP1

signal, and both of their values increase robustly from then on. This phenomenon can be attributed to the deterioration of the crack, which means kurtosis and S_α have started to effectively monitor tooth damage. The developing trend of S_r is closer to those of kurtosis and S_α, however, its increasing magnitudes are much smaller compared to the other two.

It can be concluded, therefore, that RMS, FGP and FGP1 do not show indications of the presence of a tooth defect since their small upward or downward trends do not strongly suggest fault-related features. On the other hand, the behaviour of S_α and kurtosis are very similar; both reflect severe gear faults as the crack develops to 60%. Although the values of S_r also show an increase at that damage level, they do not do so to the extent that kurtosis and S_α do. Since 60% can be considered a medium or severe crack, however, for our early fault identification purpose, this result is obviously not satisfactory.

5.2 Time Domain Indices Applied to Residual Signals

The above analyses are all based on the original signal. Nevertheless, one of the core of conventional transmission diagnostic methods is the use of residual vibrational signals and corresponding fault metric for determining damage type and extent [34]. The idea of the residual signal was first proposed by Stewart [43] in 1977. For healthy gears, their gear meshing frequency and its harmonics and their shaft rotation frequency and its harmonics, which constitute the so-called regular signals dominate the meshing vibration spectrum [51]. When a local gear fault such as a crack in a tooth is present, the vibration signal in a complete revolution will be modified by the effects of a short duration impact, and then the regular components of the signal become redundant for the purpose of fault detection. Thus, in order to efficiently detect the fault features in the vibration signal, the regular components need to be removed; the rest is called the residual signal, which is supposed to be more sensitive to changes in situation.

As described in [51], currently, most gear fault diagnostic techniques are based upon the residual signal. For that reason, we, too, will apply the aforementioned statistical measures to the corresponding residual signal. In the next section, two methods of generating residual signals will be discussed. One is based on the literal definition of the residual signal given in [43], and the other is based on our own understanding.

5.2.1 Method 1 for Generating Residual Signals

Statistical methods and their performance in condition monitoring and fault detection of a planetary gearbox have been summarized in [56]. This report reveals that the residual signal not only detects the onset of damage, but also

traces its deterioration. By definition [56], the residual signal is constructed by removing the regular meshing elements which include the shaft frequencies and their harmonics, and the meshing frequencies and their harmonics. To apply this idea for our simulated signal, each set of the 1000-point original vibration data was processed utilizing a 1000-point fast Fourier Transform (FFT). Refer to Figure 4.5; the gear meshing frequency (f_m = 570Hz) and its first eight order harmonics ($2f_m$, $3f_m$, ..., $8f_m$) dominate the frequency spectrum. These eight frequency components are first eliminated from the frequency domain. As to the shaft frequency (f_1 = 30Hz), its amplitude is extremely small compared to the meshing frequency; hence, following an approach similar to that used with the meshing frequency but leaving some extra safety range, the shaft frequency and its first ten order harmonics (f_1, f_2, ..., $10f_1$) are also removed. Then applying the inverse FFT to the remaining signal, we obtain the corresponding residual signal. The procedure for deriving the residual signal is displayed in Figure 5.2, which illustrates use of the procedure when the crack level is 50%.

As can be seen, for the 50% cracked tooth, with visual observation of the plot in a time series it is possible to distinguish two significant impulses in the residual signal, but the original vibration signal is too messy for extracting useful defect features. Thus, we can infer that after the regular vibration components are removed, the residual signal carries clearer diagnostic information; this is because it has been demodulated by the direct meshing of the cracked tooth. Again, to improve the accuracy of crack detection, the statistical measurements are applied to all the residual signals.

The indicators tested in Section 5.1 are used here again and the calculation results of their changes from the healthy tooth are shown in Figure 5.3.

It can be observed that the results displayed in Figure 5.3 are similar to

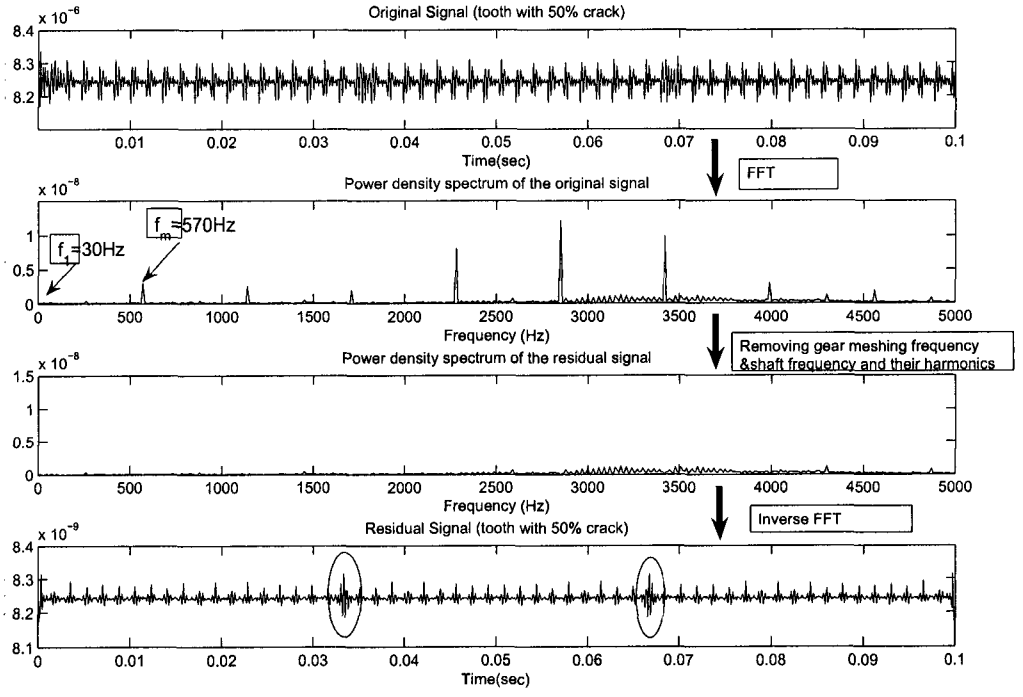

Figure 5.2: The procedure for obtaining the residual signal based on Method 1

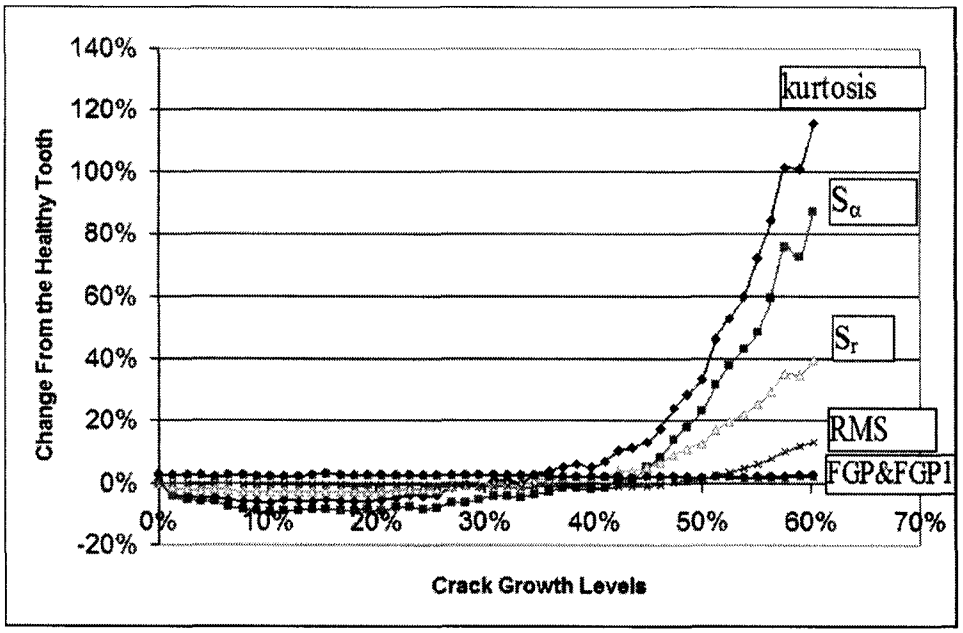

Figure 5.3: Comparison among S_α, S_r, RMS, kurtosis, FGP and FGP1 using Method 1

those in Figure 5.1. The values of FGP and FGP1 still undergo almost no change during the whole deterioration process. The values of RMS increase only slightly after the crack reaches 50%, however, the changes are too small to suggest an obvious indication of the existence of a fault. As to kurtosis and S_α, apparently, their substantial increase starts from a 45% tooth crack, a strong indication of the existence of damage. And the values of S_r also have changes due to the crack getting severe, however, the changes' magnitudes are smaller compared to kurtosis and S_α.

Since the performance of both S_α and kurtosis have proved to be better than that of other indicators, we plot their changing rate of the original and residual signals in Figure 5.4 to make the comparison clear. Because these two indicators for the residual signal start to increase more obviously from the

45% crack level and become very significant at 60%, selecting the one that reflects the damage earlier, makes it unnecessary to plot the figure after 60%. As shown in Figure 5.4, the indicator values for the original signal show almost no change in the crack range from 0% to 60%. In contrast, for the residual signal, they start to rise robustly from the 45% crack level, strongly indicating abnormal conditions in the gearbox system. We can conclude that the residual kurtosis and S_α indices reveal the existence of a fault earlier than the overall ones do.

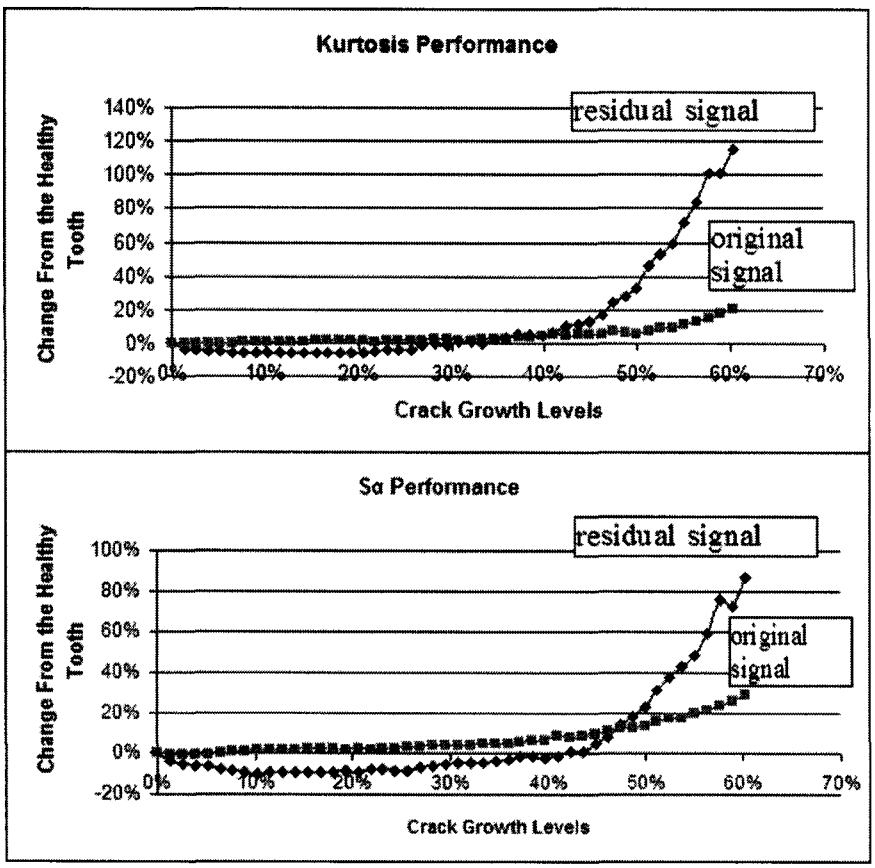

Figure 5.4: Comparison of kurtosis and S_α performance between original signals and residual signals obtained from Method 1

This approach to generating the residual signal has its own limitations to be implemented. According to the procedure we mentioned before, after eliminating the gear meshing frequency, shaft frequency and their harmonics, the inverse FFT is applied to the remaining signal. During this process, imaginary signals appear due to the algorithm of the Fourier Transform. Since the MATLAB function can treat only the real signals in our analysis, the imaginary parts are automatically ignored by the program. Although the magnitudes of the imaginary signals are 10^3 smaller than those of the real signals, some useful information must be lost through the simplification. This problem is our biggest challenge in following this method; therefore, we are searching for another simple but effective and accurate technique for generating the residual signal.

5.2.2 Method 2 for Generating Residual Signals

The another way of deriving the residual signal is demonstrated in this section. According to the definition of the residual signal, its main purpose is to remove the influence of the regular vibration components and emphasize the modulated signal induced by damage. When the gearbox is in normal working condition, all the components included in the vibration signal can be considered as regular dynamic components. Thus, if we select the normal vibration signal as a reference signal, and extract it from each set of cracked gear vibration signals, the information contained in the remaining part is all related to the gear faults.

To see the procedure for the method shown in the following example refer to Figure 5.5 in which the crack level is 50%, (a) is the original perfect gear signal, and (b) is the original 50% cracked tooth signal. We control the simulation

data so they have the same starting point and length. As a result, each data point corresponds to the same rotating angle. Thus, we simply subtract signal (a) from signal (b) and the remaining part shown in (c) is the residual signal that we are looking for.

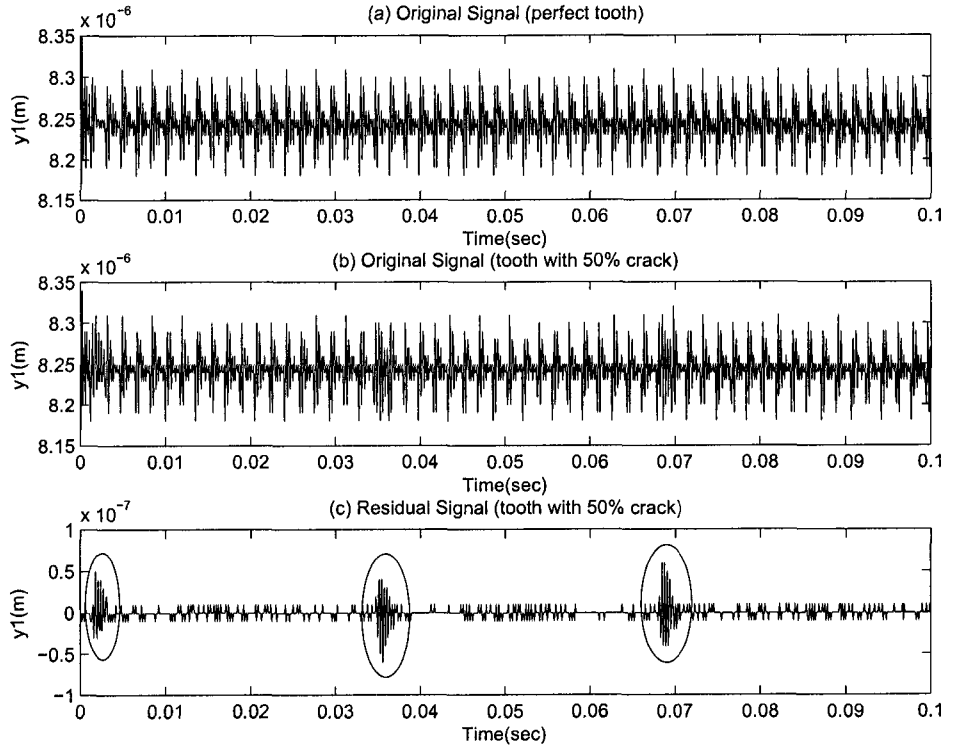

Figure 5.5: The procedure for obtaining the residual signal based on Method 2

As we expect, for the 50% cracked tooth, the periodical impulses which have been circled stand out in the residual signal while they are buried in the other vibration components in the original signal. The damage symptoms can be clearly extracted at this crack level. Thus, for small cracks whose defect features cannot be detected through visual observation, the aforementioned indicators are applied to the residual signal obtained from Method 2 and the

calculation results of their changes from the healthy tooth are shown in Figure 5.6.

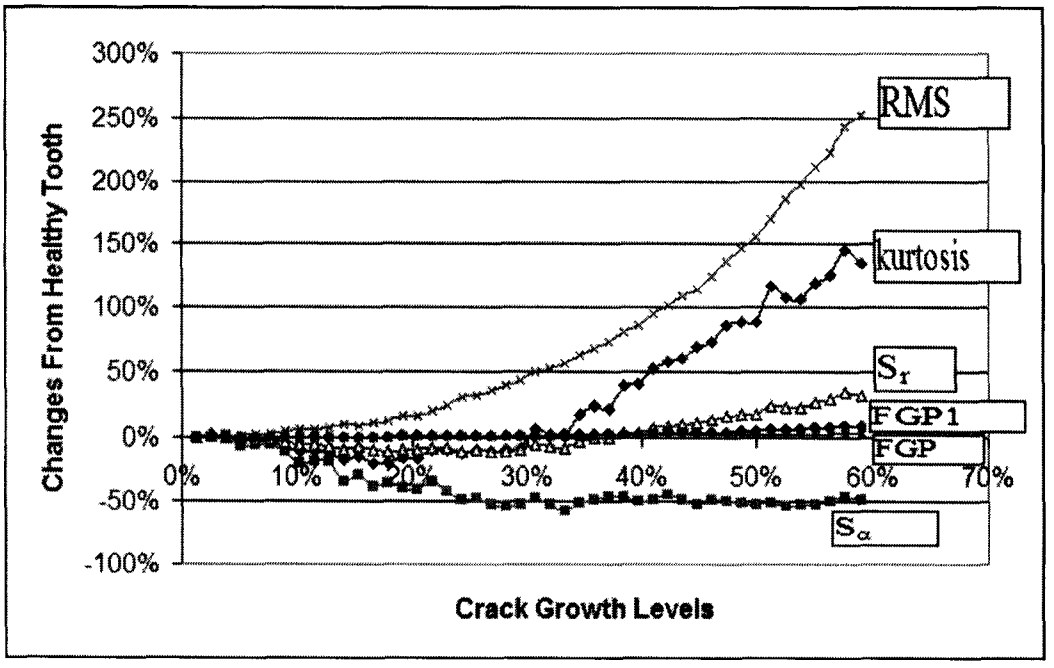

Figure 5.6: Comparison among S_α, S_r, RMS, Kurtosis, FGP and FGP1 using Method 2

As can be observed, unlike the results obtained from Method 1, there is a great difference between kurtosis and S_α. With tooth crack deterioration, the values of S_α keep decreasing rather than increasing; this makes it impossible to distinguish a difference in gear status. The mathematical explanation for such a phenomenon is that the denominator of the S_α formula increases faster than the numerator. Though the amplitude of several signal samples, $x(n)$, are enhanced due to the appearance of tooth damage, the values of S_α are still reduced. Meanwhile, it must be noted that RMS performs best under this condition. Its value starts to increase from very beginning and the increasing tendency remains in the whole crack propagation process. The reason is that

in the second method for generating residual signal, the healthy tooth signal is totally deducted, and there is no noise in the pure simulation signal, the remaining parts must be all related to the gear damages. Thus, the periodical magnitudes are strong enough to enhance the total signal average. This exactly matches the features of RMS, which is used to test the signal's average amplitude level. Therefore, RMS becomes the most sensitive one in this set of test.

On the other hand, the values of kurtosis changes also have great increasing after the crack reaches 34%. Its overall level remains constant from the incipient crack to 34%; after that, its value increases continuously. Thus the characteristics of the transients induced by the local gear faults rise from the 34% crack level through kurtosis.

After comparing all these statistical measurements in time domain, the overall performance of kurtosis emerges to be the best and most consistent. The above analyses show the robustness of kurtosis in detecting gear tooth cracks under different signal conditions. We compared the kurtosis performances under three conditions: original signal, residual signal obtained from Method 1, and residual signal obtained from Method 2. The results are shown in Figure 5.7.

According to Figure 5.7, in the crack range between 1% and 59%, the kurtosis value of residual signals obtained by Method 2 is the first one to show significant increase. Increase occurs at 34%, whereas in Method 1 it occurs at 45%, and the kurtosis values of the original signal show almost no change during the whole crack deterioration process. Comparing these conditions, kurtosis based on the residual signal obtained by Method 2 provides the earliest warning in crack recognition.

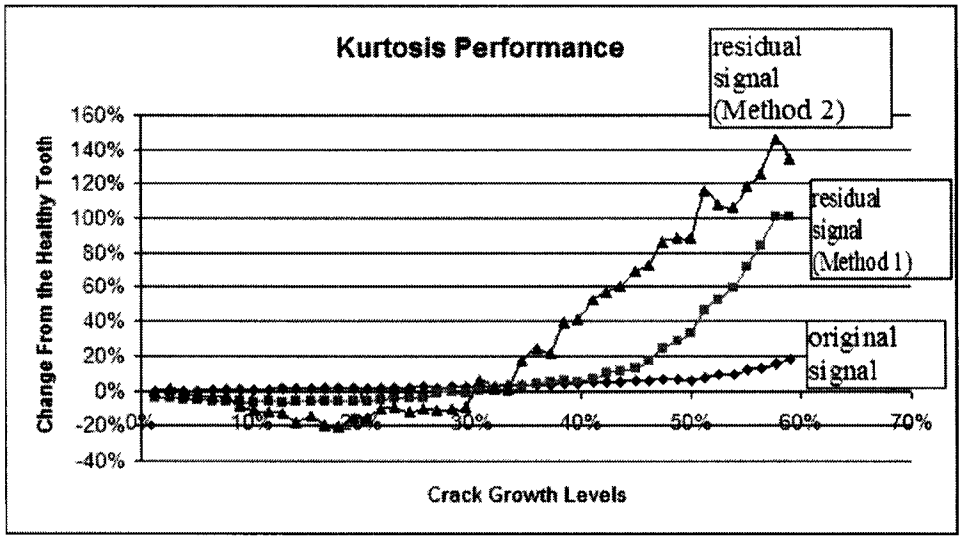

Figure 5.7: Comparison of kurtosis performance between the original signal and the residual signal obtained from Method 2

Although this method performs well in the numerically simulated data, a limitation still exists in applying it to real industry. That is, in order to implement this direct deduction approach, each set of vibration signals must serve as a synchronization signal, which means a reference signal is required to ensure that the collecting point for each set of signals will be the same. Because our analysis is based on a computer simulation, all the parameters (including the starting time and the data length) are under control. But in practical applications, it may be difficult to keep all the signals collected from the same gear rotation angle. Thus, a proximity probe must be installed to obtain an accurate reference signal and indicate the start of each new revolution. Because it is often impossible to obtain such reference signals in practical applications [32], intensive investigation still needs to be conducted.

5.3 Frequency Domain Indices Applied to Original Signals

After testing these currently existing statistical indicators, kurtosis emerges as the most effective tool; it can consistently identify fatigue tooth cracks from different deterioration levels. Based on its robust and reliable performance, the following study focuses on this statistical measurement.

Kurtosis is a measure of whether the data are peaked or flat relative to a normal distribution [35], which some physicists call a Gaussian distribution. As described in [11], when the signal is applied to a Gaussian distribution, its kurtosis value must be around 3. Moreover, in most cases, a kurtosis value greater than 3 indicates a peaked distribution; in contrast, a kurtosis value of less than 3 indicates a flat distribution. Therefore, kurtosis is considered an indicator of a signal's Gaussianity. Since the existence of a crack in a gearbox is seen as a factor that shifts a vibration signal towards non-Gaussian behaviour [18], kurtosis can be used to identify the changes in signals caused by this kind of defect.

Based on our aforementioned analysis in Section 5.1, when a gear tooth is in normal condition at the 0% crack level, its corresponding kurtosis value is 3.14, which is an acceptable value for the Gaussian distribution because it is very close to the expected value of 3. Then, as a crack starts and propagates, the vibration signatures gradually shift to non-Gaussian behaviour, and kurtosis values increase far beyond the nominal value of 3. For example, when a crack propagates to 79%, its corresponding kurtosis value is 6.46, which indicates considerable peakedness compared to the Gaussian distribution. Since many tests using time-domain kurtosis have been performed in the pervious two sections, the application of frequency-domain kurtosis will be our next objective.

A so-called "Spectral Kurtosis" (SK) was proposed by Dwyer [10] in 1983. It is a statistical tool which can indicate the presence of series of transients and determine their locations in the frequency domain. The significant advantage of Spectral Kurtosis is that "it can indicate not only non-Gaussian components in a signal, but also their locations in the frequency domain"[3]. Spectral Kurtosis was originally developed to detect randomly occurring and highly impulsive ambient noise signals under ice.

Spectral Kurtosis was proposed as a supplement for the traditional frequency-domain analysis tool – Power Spectral Density (PSD). The Power Spectrum Density (PSD) estimation is a very general basis for fault detection in vibration analysis. PSD is essentially a sum of the estimates of the second-order moments for both the real and imaginary parts of each frequency component in the frequency domain [12]. Assume there are n sets of vibration signals in total, for the ith dataset, the corresponding spectrum magnitude for a particular frequency component, F_p, is $X(i, F_p)$. Then, the power spectrum density (PSD) estimate is defined as [11]:

$$P(F_p) = \frac{1}{n}\sum_{i=1}^{n} X(i, F_p)X^*(i, F_p) \tag{5.5}$$

where the asterisk designates a complex conjugate. Although the estimation of power spectral density is a well-known and often employed method in conventional signal-processing applications, the main disadvantage of PSD is that it always averages the energy contained in the vibration response. From Equation (5.5), we see that the procedure for calculating PSD is one of summation and averaging. Even though several dominant frequency components have relatively high spectrum magnitudes, their outlier contributions can be masked through the average. As has been illustrated in Figures 4.9 and 4.10, a pure

power spectral density analysis does not lead to an accurate indication of gear damage until the crack grows to a severe level (78% in the above analysis). Under such circumstance, Spectral Kurtosis was developed to test the consistency of the magnitudes of each frequency component so as to detect unexpected outliers.

In [11], the Spectral Kurtosis was used to estimate the signal contaminated by the high impulsive and randomly occurring under ice noise, which means distinguishing Gaussian signals from ice sounds. For a Gaussian distribution, kurtosis will have a value around 3 within some confidence bounds. Due to the occurrence of the under ice ambient noise produced by ice dynamics, some frequency components would be modulated and the FFT output could exhibit non-Gaussian behaviour. Then, use a high order moment, – kurtosis of the frequency components, the non Gaussian distributed frequency domain signals can be easily detected. The kurtosis was defined in the frequency domain as [11]:

$$K(F_p) = \frac{\frac{1}{n}\sum_{i=1}^{n}[X(i,F_p)]^4}{(\frac{1}{n}\sum_{i=1}^{n}[X(i,F_p)]^2)^2}. \tag{5.6}$$

Fast Fourier transform (FFT) is used to process the collected data, and the Spectral Kurtosis estimation for the FFT output versus frequency is plotted. If at many frequency locations, the Spectral Kurtosis values deviate significantly from the value of 3, it indicates the location of non-Gaussian signals.

Since tooth root crack can be considered as a factor that shift the vibration signal to the non-Gaussian behaviour, the principle of Spectral Kurtosis may be applicable to our crack-recognition purpose. The algorithm of SK detects those modulated frequency components that may be attributed to the initiation and evolution of the tooth crack inside the gearbox. The occurrence of

unexpected damage will produce transient peaks in the vibration signal which may cause wide fluctuations at several frequencies of the vibration spectrum; it is anticipated that the use of SK will identify these components. For that reason, in this thesis, Spectral Kurtosis will be tested for vibration-based diagnostics.

Through our computer simulation, we have already obtained dozens of vibration datasets at different crack levels. Select the datasets from the perfect gear tooth condition (when the corresponding crack length is $q = 0$) to the 50% cracked gear tooth condition (when the corresponding crack length is $q = 3.9$mm). Since the incremental crack size is 0.1mm, the total number of datasets is $n = 40$. Since each dataset (ith) includes 1000 data points, utilize a 1000-point fast Fourier transform(FFT) to obtain $X(i, F_p)$. Since there are a total of 1000 points in 0.1sec, the sampling frequency is 1/0.0001. Then, after FFT, for each dataset's spectrum, the studied frequency range (i.e. the range of F_p) is between 0Hz and 5000Hz, the interval between each two adjacent frequency components is equal to 10Hz. Repeat the procedure for all the 40 datasets, then, the Spectral Kurtosis of the 40 datasets at different frequency components, F_p, is calculated according to Equation (5.6) and the results are shown in Figure 5.8.

As observed from Figure 5.8, most frequencies' kurtosis values are lower than 3, which means the distribution of spectra at most frequencies is very flat compared to the Gaussian distribution. Nevertheless, there are still three outliers in the plot. These three frequency components are 2970Hz, 3000Hz and 3060Hz respectively, and their corresponding SK values are 6.04, 4.12 and 4.66. These peaks distinguish the outlier from normal distribution; they can be related to transient impulses in the vibration signal.

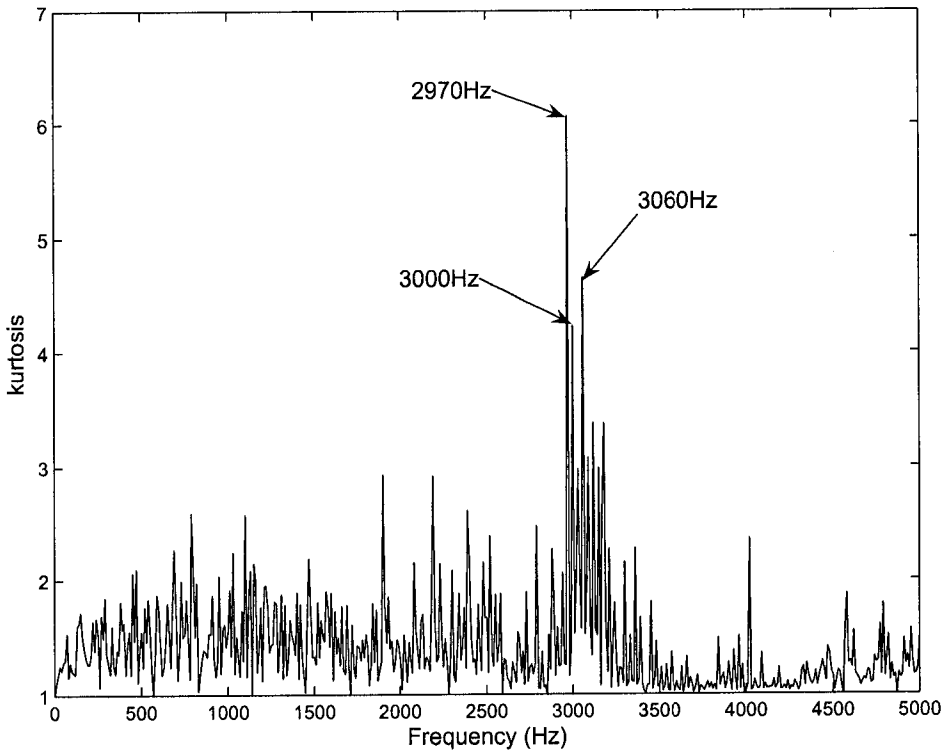

Figure 5.8: Spectral Kurtosis

It is during the calculation process that the main drawback of SK is noticed, i.e., it cannot reflect the evolution of the gear damage. As shown in Figure 5.8, it represents the gear conditions from the 0% to the 50% crack levels on a plot, but it cannot reflect the tooth condition at each damage level. As a result, we expect to develop an indicator that can be calculated at each crack level, so that, through comparing the different levels' index values, it will be possible to track the whole fault deterioration process.

Referring to the analyses in Section 5.1, we see that FGP also tries to distinguish the outliers from the normal distribution. It is supposed that the perfect gear vibration signal is applied to the normal distribution. Then, 99.7% of the data points remain within three deviations. For a signal collected from an unknown health condition, if a high percentage of the data points lie outside of three deviations, the signal must be more peaked than the normal distribution; this can be attributed to damage inside the gearbox. Based on the testing results in Sections 5.1 and 5.2, it has been demonstrated that FGP does not perform very well in the time domain. Thus, for the similar principles of FGP and Spectral Kurtosis, in the following, we will apply FGP to the frequency domain signals. The important thing is constituting the baseline conditions with perfect gear pairs first. The baseline is composed of several vibration signals which are collected under perfect gear conditions. Then, repeatedly, a set vibration signal is selected and collected under unknown gear conditions for comparison with the baseline. By comparing the unknown with the perfect, it is possible to distinguish the health condition of the unknown signal. The procedure is described in detail as follows:

- In the computer simulation, when all the parameters' values are fixed, only one normal condition gear vibration signal can be obtained. Since a

series of vibration signals are required for the baseline datasets, a tooth with a microstructurally small crack (from 0.1%, 0.2%, ..., 0.9%) is considered to be working normally. Then, the normal vibration signal and nine increments of crack levels up to 0.9% (making a total of ten datasets) constitute the baseline.

- Use "FFT" algorithm to transform each of these ten signals from the time domain to the frequency domain. As shown in Figure 5.9, at each frequency component F_p (one of the dominant frequency components is circled as an example), there are ten spectrum magnitudes in total.

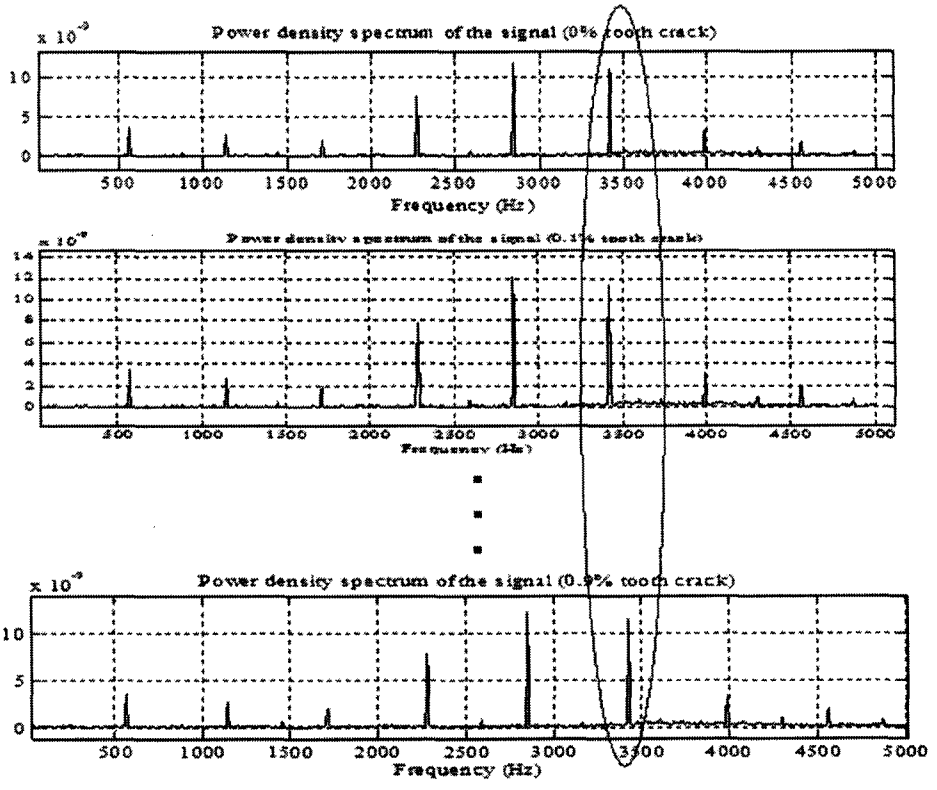

Figure 5.9: Baseline datasets in the frequency domain

- For each frequency component, calculate its Spectral Kurtosis according to Equation (5.6). As displayed in Figure 5.10, at most frequency bins, the SK values are significantly lower than 3, which indicates a flat distribution. Only at 1860Hz, the SK value is 3.647, slightly over 3.5; however, this is still within the error tolerance that can be attributed to error generated from the numerical simulation. Therefore, from Figure 5.10, it can be seen that when all the gear teeth are in perfect operating condition, their vibration spectra are less peaked than the Gaussian distribution.

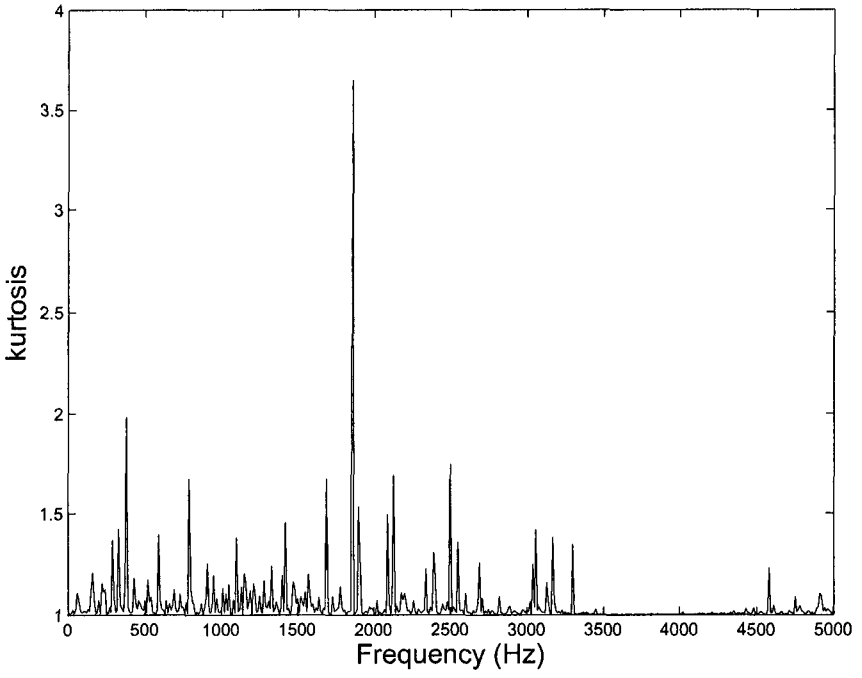

Figure 5.10: Spectral Kurtosis of the baseline

- Calculate the mean value and the standard deviation of the ten spectrum magnitudes as the baseline mean value, $\bar{r}$, and baseline standard

deviation, σ_0, at each frequency cell. The results are displayed in Figure 5.11. For the Gaussian distribution, 99.7% of the data points remain within three standard deviations. At each frequency, compare the ten spectrum magnitudes with the baseline mean value and three standard deviations, $\bar{r} + 3\sigma_0$, respectively; all the magnitudes remain in the range of $\bar{r} + 3\sigma_0$. This result corroborates the information contained in Figure 5.10 that the vibration spectra of perfect gear teeth are less peaked than the Gaussian distribution.

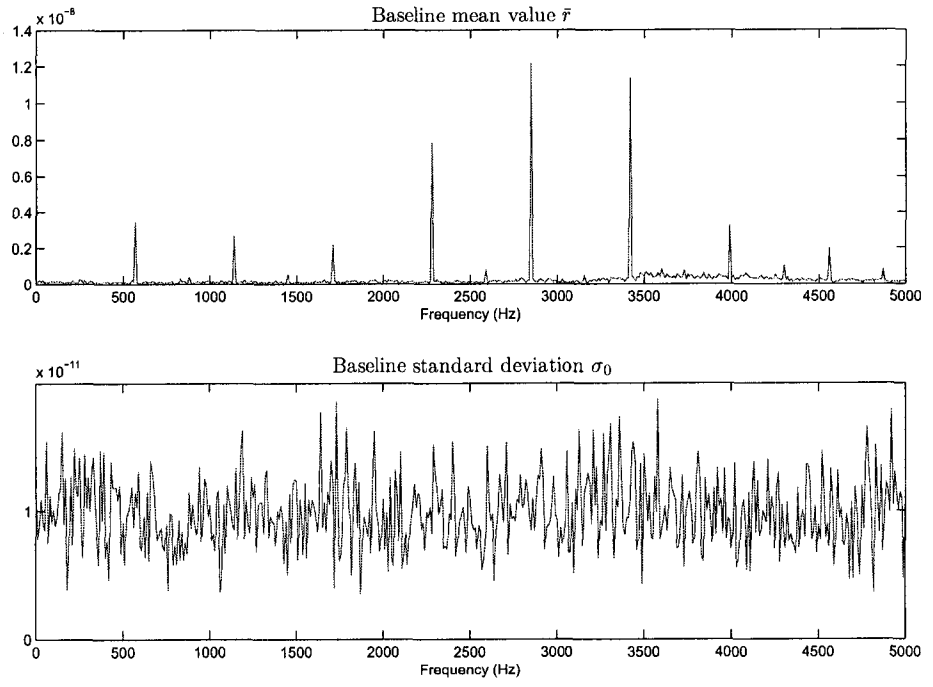

Figure 5.11: Baseline's $\bar{r}$ and σ_0

- Select a cracked gear tooth signal; again apply "FFT" to transform the time domain signal to the frequency domain. As above, for each fre-

quency cell, there is a related spectrum magnitude. Compare it with the baseline mean value, $\bar{r}$, to test whether its value is greater than $\bar{r} + 3\sigma_0$ or not. Thus, if the value is greater than $\bar{r} + 3\sigma_0$, this point is considered an outlier to the Gaussian distribution. Since our purpose is to calculate the number of these outliers, for each frequency with a spectrum magnitude greater than $\bar{r} + 3\sigma_0$, record the number as 1, otherwise, record the number as 0.

- In our calculation, there are a total of 500 frequency components in the frequency spectrum. Each component has a value of either 1 or 0, which represents whether this point is an outlier of the Gaussian distribution or not. Add all these numbers together, and divide by the total number, 500; the result indicates the percentage of the outliers in the frequency domain.

- Change to a different crack level vibration signal and repeat the same procedure. When done, each condition has its own percentage value, which relates to the health of the gearbox.

Plot these percentage values with the crack deterioration levels; the results are shown in Figure 5.12. From this plot, crack evolution is clearly demonstrated through the indicator's developing trend. For the perfect gear tooth condition, the frequency spectra are less peaked than the Gaussian distribution, so no outliers can be detected. Then, the tooth root crack starts to appear. In the initial crack period, the percentage of outliers increases significantly, rising from 4% to 32%. With the propagation of the tooth crack, after the crack has developed to 23%, the percentage of outliers remains at a high level (around 36%) with little variation. Therefore, we conclude that this

approach is very sensitive to fault identification in the early stage. When the crack is first present, the numbers of outliers in the frequency domain increases rapidly, clearly indicating the abnormal condition inside the gearbox. After a period of time, however, the trend of the development of outliers flattens, suggesting the crack is propagating to the medium and severe levels. Refer to the other results of statistical analysis as shown in Figure 5.7; their values remain at a constant level in the initial crack period; this means these techniques reflect fault conditions only when a crack grows to the medium or severe level. Whereas the frequency domain, FGP, shows its high sensitivity to the initial fault as its values rise dramatically before the crack reaches 23%. Thus, by comparing Figures 5.12 and 5.7, it can be concluded that the improved statistic approach applied in the frequency domain can effectively distinguish cracked gear tooth signatures from normal vibration signatures at an early stage.

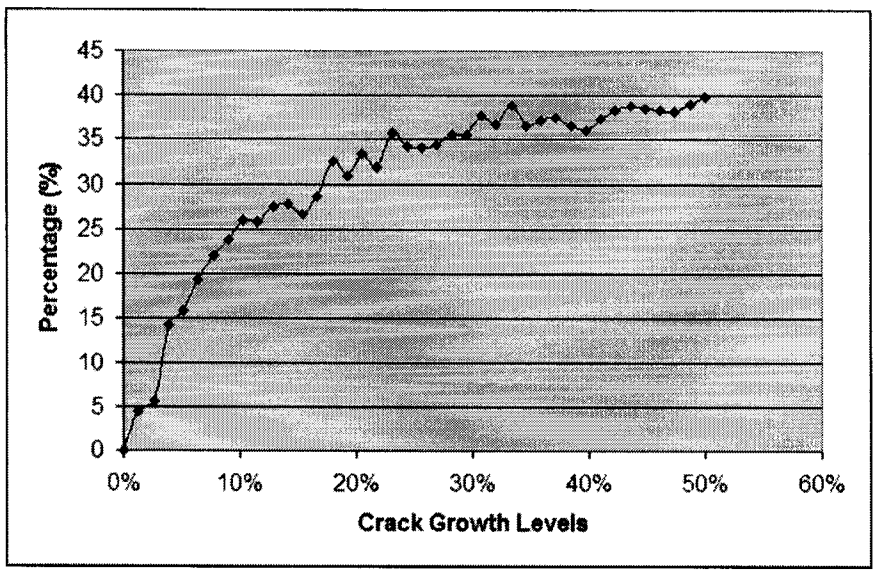

Figure 5.12: Frequency domain FGP

5.4 General Discussion

In this chapter, we investigated various statistic indicators based on our simulated vibration signals in both the time and frequency domains. We have concluded that among the studied statistical measurements, kurtosis is the most effective and robust time domain indicator in identifying tooth root cracks, especially for the residual signal obtained from Method 2; however, this index only starts to work at the medium or severe damage level. Then, from the concept of Spectral Kurtosis, a time domain indicator, FGP, is improved by being applied to the frequency domain signal, which has been found to be very sensitive to initial gear damage. These techniques have been compared, and their pros and cons are summarized in the following table:

Table 5.1: Comparison among different analyses

	Pros	Cons
Time domain indices applied to the original signal	Simple to apply	Too late for early crack detection purpose (indicates the existence of crack at 60% level)
Time domain indices applied to the residual signal obtained from Method 1	Detects crack earlier than 50%	Imaginary signals are ignored during calculation, decreasing the accuracy of the residual signal
Time domain indices applied to the residual signal obtained from Method 2	Detects crack earlier than 35%	Need to install a proximity probe in the real experiment signals
Frequency domain FGP	Very sensitive to incipient cracks	Needs to be tested on real experiment signals

A couple observation of the studies reported in this Chapter deserve some attention here. First, we used approximately 3.3 revolutions of the pinion shaft to compute the indicators. We may get more accurate indicators if an integer number of revolutions is used instead. The second observation is related to

the Spectral Kurtosis method. The expected kurtosis value at each frequency band when the pinion is perfect may be a value different from 3. Additional investigations on these observations will be conducted in the future.

Chapter 6

Conclusions and Future Work

This thesis studies through computer simulation the effects of tooth crack on the vibration response of a one-stage gearbox with spur gears. An involute pair of meshing spur gears consisting of a perfect gear and a pinion with a cracked tooth have been presented. A pinion with fatigue cracks varying from 0% to 80% of the tooth root was first introduced. An analytic model for describing gear total mesh stiffness with perfect or cracked gear teeth is then applied and the numeric results are inserted into a lumped parameter model to simulate the vibration response of gears under different deterioration levels of tooth crack.

In order to find a simple and effective technique to distinguish a crack from a normal condition, a number of tests based on signal kurtosis and other statistical measurements are applied to the numerically-generated time series vibration signals. By comparing these methods, we learn which technique is the most effective in gearbox fault diagnosis. As well, a new indicator is improved based on existing frequency domain statistic measurements; it is especially sensitive to the initial tooth crack.

After being applied to the original time domain signal, residual time domain

signal and frequency domain signal, the conventional indicator, "kurtosis", is proved to be more reliable and sensitive than the other statistical moments in detecting the short period impact induced by gear faults.

The residual signal whose regular vibration components have been removed carries clearer diagnostic information than does the original signal; however, difficulties remain in generating an accurate residual signal. When using the literal definition developed by [43] in generating residual signals, imaginary signals will appear; they are ignored in our studies. An alternative method is also applied to obtaining the residual signal; it is simple to implement when using simulation data. On the other hand, for real experiments, a proximity probe needs to be installed; this is not often possible in practical applications.

The improved FGP based on the frequency domain shows its effectiveness in fault detection. Its values rise significantly for an incipient crack, and the developing trend flattens with the propagation of the tooth damage. Although there is still no full agreement on the criteria for strictly determining whether there a fault exists or not, the improved FGP performs well in giving an early warning of a crack's existence.

The signatures simulated in this thesis will be useful in testing other advanced signal processing methods and early fault-detection techniques. Furthermore, the results presented in this study will also be useful for characterization of the fault signatures generated by cracks in gearboxes. They can be used to define the signatures of tooth crack in gearboxes.

As a result, possible future research can be summarized as dealing with the following aspects: the inner friction force of teeth in the dynamic model which this study ignored for the purpose of simplification; the simulation of more vibration signals from other kinds of gear faults for comparison with

gear tooth cracks, new techniques that can identify different kinds of gear damage, adding noise to pure simulation data in order to make it more similar to reality, utilizing the de-noising signal processing method in connection with the above statistical measurements; and field-testing the improved FGP. The improved FGP performs successfully in working with numerically simulated data, nevertheless, the signals collected from lab experiments or the field are also necessary to test its robustness and reliability in the real world of industry.

BIBLIOGRAPHY

[1] Cepstrum. *http://en.wikipedia.org/wiki/Cepstrum*, June, 2006.

[2] F.A. Andrade, I.I. Esat, and M.N.M. Badi. Gear condition monitoring by a new application of the kolmogorov-smirnov test. *Journal of Mechanical Engineering Science*, 215(6), 2001.

[3] J. Antoni. The spectral kurtosis: a useful tool for characterising non-stationary signals. *Mechanical Systems and Signal Processing*, 20:282–307, 2006.

[4] W. Bartelmus. Mathematical modelling and computer simulations as an aid to gearbox diagnostics. *Mechanical Systems and Signal Processing*, 15(5):855–871, 2001.

[5] N. Baydar and A. Ball. Detection of gear failures via vibration and acoustic signals using wavelet transform. *Mechanical Systems and Signal Processing*, 17(4), 2003.

[6] T. Bose. *Digital signal and image processing.* J. Wiley, 2004.

[7] A. Cowie. The kinematics of contacting surfaces. *Journal of Engineering for Industry*, pages 450–454, 1968.

[8] L.T. DeCarlo. On the meaning and use of kurtosis. *Psychological Methods*, 2(3), 1997.

[9] J.P. Dron, F. Bolaers, and I. Rasolofondraibe. Improvement of the sensitivity of the scalar indicators (crest factor, kurtosis) using a de-noising method by spectral substraction: application to the detection of defects in ball bearings. *Journal of Sound and Vibration*, 270(1-2):61–73, 2004.

[10] R.F Dwyer. Detection of non-gaussian signals by frequency domain kurtosis estimation. *IEEE ICASSP-83 Conv. Rec.*, pages 607–610, 1983.

[11] R.F Dwyer. A technique for improving detection and estimation of signals contaminated by under ice noise. *J.Acoust.Soc.Am*, 74(1):124–130, 1983.

[12] R.F Dwyer. Use of the kurtosis statistic in the frequency domain as an aid in detecting random signals. *IEEE Journal of Oceanic Engineering*, OE-9(2), April 1984.

[13] D. Dyer and R.M. Stewart. Detection of rolling element bearing damage by statistical vibration analysis. *Transactions of the ASME, Journal of Mechanical Design*, 100(2), 1978.

[14] T. Fakhfakh, F. Chaari, and M. Haddar. Numerical and experimental analysis of a gear system with teeth defects. *Int J Adv Manuf Technol*, 25:542–550, 2005.

[15] A. Flodin and S. Andersson. Simulation of mild wear in spur gears. *Wear*, 207:16–23, 1997.

[16] B.D. Forrester. *Advanced vibration analysis techniques for fault detection and diagnosis in geared transmission systems.* PhD thesis, Swinburne University of Technology, 1996.

[17] R.G.E. Franks. *Modeling and simulation in chemical engineering.* John Wiley & Sons, Inc., 1972.

[18] L.J. Hadjileontiadis, E. Douka, and A. Trochidis. Crack detection in beams using kurtosis. *Computers and Structures*, 83:909–919, 2005.

[19] J.K. Hammond and P.R. White. The analysis of non-stationary signals using time-frequency methods. *Journal of Sound and Vibration*, 190(3), 1996.

[20] F. Honarvar and H.R. Marin. New statistical moments for diagnositics of rolling element bearings. *Journal of Manufacturing Science and Engineering*, 119:425–432, 1997.

[21] I. Howard, S.X. Jia, and J.D. Wang. The dynamic modelling of a spur gear in mesh including friction and a crack. *Mechanical Systems and Signal Processing*, 15(5):831–853, 2001.

[22] D.T. Jelaska, S. Glodez, J. Kramberger, and S. Podrug. Numerical modelling of the crack propagation path at gear tooth root. *Proceedings of the ASME Design Engineering Technical Conference*, v4A:201–207, 2003.

[23] R. Kasuba and J.W. Evans. An extended model for determining dynamic loads in spur gearing. *Journal of Mechanical Design, Transactions of the American Society of Mechanical Engineers*, 103:398–409, 1981.

[24] J. Kramberger, M. Sraml, S. Glodez, J. Flasker, and I. Potrc. Computational model for the analysis of bending fatigue in gears. *Computers and Structures*, 82(23-26), 2004.

[25] J.H. Kuang and A.D. Lin. The effect of tooth wear on the vibration spectrum of a spur gear pair. *Journal of Vibration and Acoustics*, 123(3):311–317, 2001.

[26] A.S. Kumar, T.S. Sankar, and M.O.M. Osman. On dynamic tooth load and stability of a spur-gear system using the state-space approach. *Journal of Mechanisms, Transmissions, and Automation in Design, Transactions of the American Society of Mechanical Engineers*, 107:54–60, 1985.

[27] W.X. Lai, P.W. Tse, G.C. Zhang, and T.L. Shi. Classification of gear faults using cumulants and the radial basis function network. *Mechanical Systems and Signal Processing*, 18(2), 2004.

[28] D.G. Lewicki. Gear crack propagation path studies – guidelines for ultra-safe design. *Journal of the American Helicopter Society*, 47(1), 2002.

[29] C.J. Li, H. Lee, and S.H. Choi. Estimating size of gear tooth root crack using embedded modelling. *Mechanical Systems and Signal Processing*, 16(5), 2002.

[30] C.J. Li and J.D. Limmer. Model-based condition index for tracking gear wear and fatigue damage. *Wear*, 241:26–32, 2000.

[31] D. Lin, M. Wiseman, D. Banjevic, and A.K.S. Jardine. An approach to signal processing and condition-based maintenance for gearboxes subject to tooth failure. *Mechanical Systems and Signal Processing*, 18(5), 2004.

[32] J. Lin and M.J. Zuo. Gearbox fault diagnosis using adaptive wavelet filter. *Mechanical Systems and Signal Processing*, 17(6), 2003.

[33] S.T. Lin and P.D. McFadden. Gear vibration analysis by b-spline wavelet-based linear wavelet transform. *Mechanical Systems and Signal Processing*, 11(4), 1997.

[34] L. Liu. The influence of gear design parameters on gear tooth damage detection sensitivity. *Journal of Mechanical Design, Transactions of the ASME*, 124(4), 2002.

[35] T. Lokajicek and K. Klima. A first arrival identification system of acoustic emission(ae) signals by means of a high-order statistics approach. *Measurement Science and Technology*, 17:2461–2466, 2006.

[36] S. Loutridis, E. Douka, and L.J. Hadjileontiadis. Forced vibration behaviour and crack detection of cracked beams using instantaneous frequency. *NDT & E International*, 38(5), 2005.

[37] MathWorks. *MATLAB User's Guide.* The MathWorks, Inc., 1996.

[38] G. Meltzer and N.P. Dien. Fault diagnosis in gears operating under non-stationary rotational speed using polar wavelet amplitude maps. *Mechanical Systems and Signal Processing*, 18(5), 2004.

[39] A.J. Miller. A new wavelet basis for the decomposition of gear motion error signals and its application to gearbox diagnostics. Master's thesis, Pennsylvania State University, 1999.

[40] T. Nakada and M. Utagawa. Dynamic loads caused by the varying elasticity of mating gear teeth. *Proceddings of the 6th Japan National Congress on Applied Mechanics*, pages 493–497, 1956.

[41] R.B. Randall. *Frequency analysis*, volume 3rd edition. Bruel and Kjar, Copenhagen, 1987.

[42] V.B. Rao. Kurtosis as a metric in the assessment of gear damage. *The Shock and Vibration Digest*, 31(6):443–448, 1999.

[43] R.M. Stewart. Some useful data analysis techniques for gearbox diagnostics. *Applications of Time Series Analysis. ISVR, University of Southampton*, 1977.

[44] B. Tao, L. M. Zhu, H. Ding, and Y. L. Xiong. An alternative diagnostic index of rolling element bearings – a comparison study. In Press.

[45] X.H. Tian. Dynamic simulation for system response of gearbox including localized gear faults. Master's thesis, University of Alberta, 2004.

[46] M. Utagawa. Dynamic loads on spur gear teeth. *Bulletin of Japanese Society of Mechanical Engineers*, 1(4):397–403, 1958.

[47] A. Versicherungs. *Handbook of loss prevention.* Springer-Verlag, Berlin, 1978.

[48] W.J. Wang and P.D. McFadden. Early detection of gear failure by vibration analysis.1.calculation of the time-frequency distribution. *Mechanical Systems and Signal Processing*, 7(3), 1993.

[49] W.J. Wang and P.D. McFadden. Application of wavelets to gearbox vibration signals for fault detection. *Journal of Sound and Vibration*, 192(5), 1996.

[50] W.Q. Wang, F. Ismail, and M.F. Golnaraghi. Assessment of gear damage monitoring techniques using vibration measurements. *Mechanical Systems and Signal Processing*, 15(5), 2001.

[51] W.Y. Wang. Early detection of gear tooth cracking using the resonance demodulation technique. *Mechanical Systems and Signal Processing*, 15(5), 2001.

[52] D.C.H. Yang and J.Y. Lin. Hertzian damping, tooth friction and bending elasticity in gear impact dynamics. *Journal of Mechanisms, Transmissions, and Automation in Design*, 109(2), 1987.

[53] D.C.H. Yang and Z.S. Sun. A rotary model for spur gear dynamics. *ASME Journal of Mechanisms, Transmissions, and Automation in Design*, 85-DET-2:7p, 1985.

[54] Z. Yang and Z.H. Sheng. Condition monitoring and diagnostics for rotating machinery using artificial neural networks. *Journal of Southeast University*, 13(2):54–60, 1997.

[55] I. Yesilyurt, F.S. Gu, and A.D. Ball. Gear tooth stiffness reduction measurement using modal analysis and its use in wear fault severity assessment of spur gears. *NDT & E International*, 36(5), 2003.

[56] M.J. Zuo and W. Li. Statistical methods for low speed planetary gearbox monitoring. Technical report, Department of Mechanical Engineering, University of Alberta, 2005.